

Review

Recent Trends in Metal Nanoparticles Decorated 2D Materials for Electrochemical Biomarker Detection

Aneesh Koyappayil [†], Ajay Kumar Yagati [†] and Min-Ho Lee ^{*†}

School of Integrative Engineering, Chung-Ang University, 84 Heuseok-ro, Dongjak-Gu, Seoul 06974, Republic of Korea

* Correspondence: mhlee7@cau.ac.kr; Tel.: +82-2-820-5503; Fax: +82-2-814-2651

† These authors contributed equally to this work.

Abstract: Technological advancements in the healthcare sector have pushed for improved sensors and devices for disease diagnosis and treatment. Recently, with the discovery of numerous biomarkers for various specific physiological conditions, early disease screening has become a possibility. Biomarkers are the body's early warning systems, which are indicators of a biological state that provides a standardized and precise way of evaluating the progression of disease or infection. Owing to the extremely low concentrations of various biomarkers in bodily fluids, signal amplification strategies have become crucial for the detection of biomarkers. Metal nanoparticles are commonly applied on 2D platforms to anchor antibodies and enhance the signals for electrochemical biomarker detection. In this context, this review will discuss the recent trends and advances in metal nanoparticle decorated 2D materials for electrochemical biomarker detection. The prospects, advantages, and limitations of this strategy also will be discussed in the concluding section of this review.

Keywords: metal nanoparticles; immunosensor; MXene; MoS₂; graphene; MOF; biomarkers; graphitic carbon nitride; black phosphorous; 2D-LDHs; boron nitrides; graphdiyne

1. Introduction

The definition of biomarkers has evolved over time, and a broader definition was suggested by the World Health Organization as “a biomarker is any substance, structure, or process that can be measured in the body or its products and influence or predict the incidence of outcome or disease” [1,2]. More specific definitions such as “a biological molecule found in blood, other body fluids, or tissues that is a sign of a normal or abnormal process, or of a condition or disease and can be tested to see how well the body responds to treatment for a disease or condition” [3], and “a characteristic that can be objectively measured and quantitatively evaluated as an indicator of a normal biological and pathological process, or pharmacological responses to a therapeutic intervention” [4] were coined by the US National Cancer Institute, and the US National Institutes of Health, respectively. Biomarkers can be biological, chemical, or physical, and are measurable parameters indicative of a specific biological state. The detection of biomarkers is crucial for the diagnosis and treatment of numerous diseases [5]. Biomarkers are classified broadly into imaging biomarkers and molecular biomarkers based on their characteristics. Imaging biomarkers are often used in combination with various imaging tools, whereas molecular biomarkers comprise RNA, DNA, and proteins [6]. Molecular biomarkers are easily quantifiable from biological samples and can complement clinical characteristics [7,8]. Another category, known as pharmacodynamic biomarkers, is applied in drug development during dose optimization studies [9]. Based on the application, biomarkers are classified into prognostic biomarkers, diagnostic biomarkers, predictive biomarkers, and monitoring biomarkers [10]. Prognostic biomarkers help to identify the risk of disease progression in the future [11]. Diagnostic biomarkers help physicians to identify a specific disease condition [12], and predictive biomarkers predict the responses related to therapeutic interventions [11], whereas



Citation: Koyappayil, A.; Yagati, A.K.; Lee, M.-H. Recent Trends in Metal Nanoparticles Decorated 2D Materials for Electrochemical Biomarker Detection. *Biosensors* **2023**, *13*, 91. <https://doi.org/10.3390/bios13010091>

Received: 7 November 2022

Revised: 27 December 2022

Accepted: 1 January 2023

Published: 5 January 2023



Copyright: © 2023 by the authors. Licensee MDPI, Basel, Switzerland. This article is an open access article distributed under the terms and conditions of the Creative Commons Attribution (CC BY) license (<https://creativecommons.org/licenses/by/4.0/>).

a monitoring biomarker is usually measured for assessing the status of a medical condition or disease [13].

An ideal biomarker sensor must capture the biomarker selectively from the complex biological matrix of interfering molecules. Although nonspecific binding is still a concern, electrochemical detection methods, specifically electrochemical impedance spectroscopy (EIS), allow the selective analysis of biomarker detections by the resistive and/or capacitive changes due to physical and/or biomolecular interactions of the electrode surfaces coated with nanomaterials, DNA, proteins, etc. [14–16]. It is one of the basic and widely used approaches to determine the fundamental redox events at the electrode-electrolyte interface. However, evaluations are made by comparing the results of the EIS with cyclic voltammetry (CV) measurements. Also, differential pulse voltammetry (DPV) and square wave voltammetry (SWV) techniques are used in biomarker detection systems for both label and label-free approaches [17,18]. Among these techniques, CV-based detection sensing is widely reported due to its ability to explain the electrochemical events, such as oxidation-reduction reactions and electron-transfer kinetics occurring at the electrode-electrolyte interface, and the mass transport towards the electrode surface [19–21]. The search for advanced functional materials for electrochemical biomarker detection has sparked a research interest in layered 2D materials over the past few years and several novel approaches were reported for the synthesis of various 2D materials and their nanocomposites with exciting immunosensor applications. The interest and demand for 2D materials have increased significantly, and the global market for 2D materials is expected to grow rapidly with a CAGR of 3.9% between 2020 and 2027 and a corresponding increase in valuation from 2.27 billion to 2.86 billion USD [22]. In this context, this review discusses the recent advances and challenges of metal nanoparticle decorated 2D materials for biomarker detection.

2. Metal Nanoparticles on 2D Materials for Biomarker Detection

Nanoparticles used separately or in conjugation with other nanomaterials on 2D materials fulfill various roles in the design and development of electrochemical immunosensors. Also, they improve the analytical characteristics of the developed sensors such as linear range, LOD, and sensitivity [23]. For instance, nanoparticles deposited on the surface of the working electrode result in an enhancement of the surface area, thereby leading to an increased molecule loading capacity [24,25]. Additionally, the unique properties of nanoparticles could enhance the signal for the sensitive determination of biomarkers [23]. Also, the high electrical conductivity of metal nanoparticles at the electrode surface accelerates the redox electron transfer process. In some cases, nanoparticles could act as platforms for anchoring antibodies [26]. Metal nanoparticles were also used as a transport medium to capture the analyte from the sample, thereby concentrating the analyte molecules towards the electrode surface to improve the analytical signal [27]. Among various metal nanoparticles, AuNPs were extensively used to immobilize antibodies on the electrode surface to effectively amplify the immunosensor signal, anchor antibodies, and improve electrocatalytic activity [28,29].

2.1. Graphene Oxide Conjugated with Nanoparticles for Electrochemical Biomarker Detection

Graphene, a single layer (monolayer) of sp^2 carbon atoms with a molecular bond length of 0.142 nm, is tightly bound in a hexagonal honeycomb lattice. It is basically extracted from graphite and is merely a sheet of graphite. Graphene possesses excellent electrical conductivity ($200,000 \text{ cm}^2/\text{Vs}$) due to its bonding and antibonding of pi orbitals, with the strongest compound around 100–130 times stronger than steel with a tensile strength of 130 GPa and a Young's Modulus of 1 TPa–150,000,000 psi. It is also one of the best conductors of heat at room temperature (at 4.84×10^3 – $5.30 \times 10^3 \text{ W/mK}$). As graphene is a subunit of graphite it can be synthesized by direct extraction from bulk graphite. From the high-quality sample of graphite, graphene can be extracted by micromechanical cleavage or the scotch tape method of production. It is a straightforward method that doesn't need any specialized equipment. A piece of adhesive tape is placed onto and then peeled off

the surface of a sample of graphite, resulting in a single to few layers of graphene. Other methods include the dispersion of graphite, exfoliation of graphite oxide, epitaxial growth, and chemical vapor deposition (CVD) as shown in Figure 1.

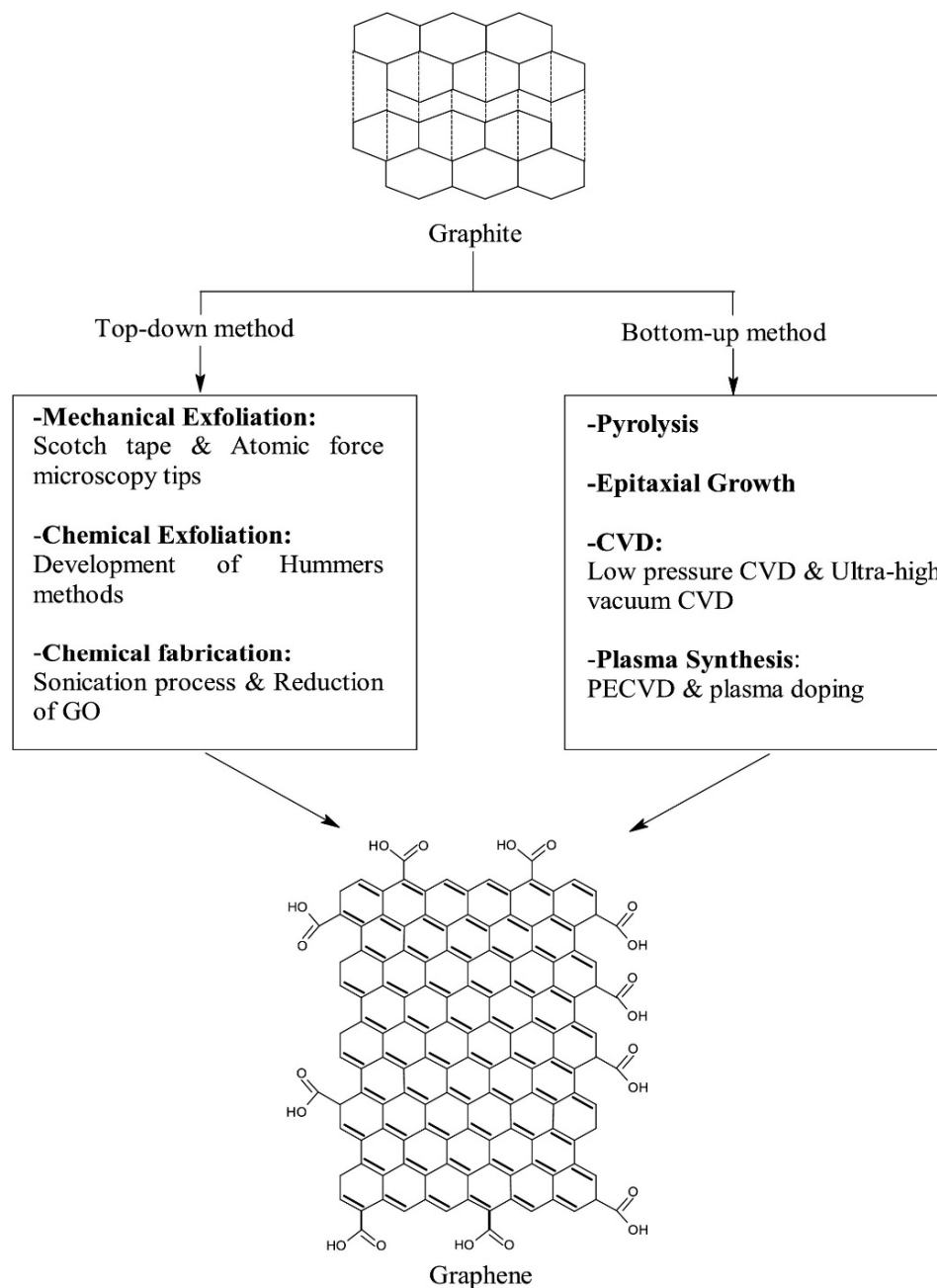


Figure 1. The schematic diagram for the synthesis of graphene. Reprinted with permission from Ref. [30]. Copyright 2018, Elsevier.

Graphene oxide is a form of graphene that includes oxygen functional groups and possesses interesting properties that are different from graphene. By reducing graphene oxide, these functional groups can be removed resulting in reduced graphene oxide. The production of reduced graphene oxide can be done in (i) chemical reduction, (ii) Thermal reduction; (iii) microwave and photoreduction; (iv) photocatalyst reduction; (v) solvothermal/hydrothermal reduction. The detailed information for various synthesis routes can be found elsewhere [31–33] and is beyond the scope of this review.

In this section, we discuss the development of various types of electrochemical sensors based on graphene oxide conjugated with nanoparticles that have been reported recently for various types of biomarkers. The development of biosensors that accurately measure the desired biomarker at high sensitivity and selectivity is crucial. However, sensitivity and selectivity are the two main factors that limit accuracy when performing the detections at the point of care with meager volumes of biological test solutions. For cancer cell analysis, the sensors should be able to detect tumors within the range of 100–1000 cell counts. To overcome these difficulties, innovative biosensor approaches with the optical, electrochemical, and piezoelectric transducer occupy the place of benchtop protocols adopted by the classical detection methods. Among these biosensors, electrochemical-based approaches competed with optical sensors which are widely used for the analysis of cancer biomarkers due to the characteristics of high sensitivity, selectivity, fast response, ease of use, low cost, and minimal fabrication procedures. In electrochemical biosensors, the right choice of transducer material is crucial, since it is the transducer that mainly influences the overall sensitivity [34] with minimal contributions from labeling methods.

Recently, Ranjan et al. [35] reported on the detection of breast cancer CD44 biomarkers using a gold-graphene oxide nanocomposite with ionic liquid with differential pulse voltammetry and electrochemical impedance spectroscopy. In this work, the authors reported the synthesis of RGO, ionic liquid (IL), and Au nanoparticles (Au NPs) by the citrate reduction method and other chemical procedures to form a nanocomposite on a glassy carbon electrode (GCE), as shown in Figure 2. In this work, the addition of 1-butyl-3-methylimidazolium tetrafluoroborate, an ionic liquid in conjugation with Au nanoparticles enabled the enhancement in the overall sensitivity of the developed sensor. Once the nanocomposite is deposited on GCE, the surface is activated with EDC/NHS to covalently bind the anti-CD44 antibodies. After the surface is blocked with BSA for nonspecific binding, then different concentrations of CD44 antigen were allowed for electrochemical investigation with CV, DPV, and EIS. The sensor possessed a linear range of 5 fg/mL to 50 µg/mL with a LOD of 2.7 fg/mL and 2.0 fg/mL in serum and PBS samples, respectively. This sensor is a promising candidate for the onsite detection of CD44 in breast cancer patients.

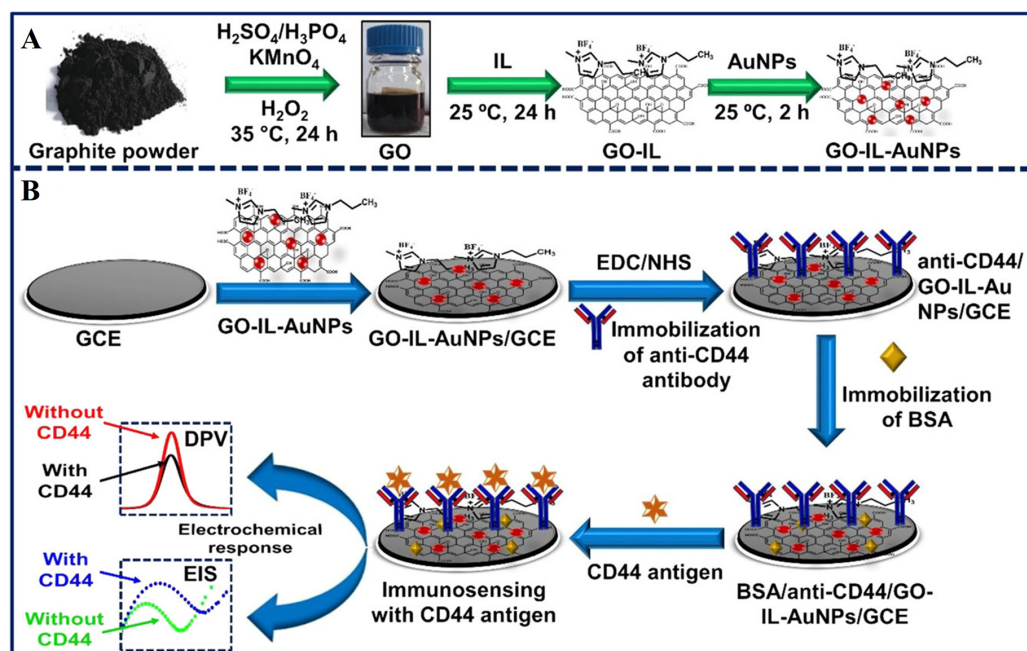


Figure 2. (A) Schematic diagram shows the synthesis of GO-IL-AuNPs hybrid nanocomposite and (B) Stepwise fabrication shows the surface modification procedures for the fabrication of BSA/anti-CD44/GO-IL-AuNPs/GCE Immunosensor. Reprinted with permission from Ref. [35] Copyright 2022, ACS.

In another study, Yagati et al. [36] proposed indium tin oxide (ITO)-based electrodes modified with reduced graphene oxide-gold nanoparticles that were used for the electrochemical impedance sensing of the C-reactive protein in serum samples. This biomarker detection is crucial in analyzing the inflammation due to an infection, and the risk of heart disease. In this study, graphene oxide-Au nanoparticles were electrodeposited on ITO microdisk electrodes fabricated using standard photolithography techniques. Subsequently, the modified electrodes were coated with a self-assembled monolayer of 3-MPA and activated with EDC/NHS. After the surface-blocking protocol was performed, then the selective antibodies were immobilized on the rGO-NP surface. Once the transducer surface is ready, a different concentration of CRP in human serum (1: 200) was detected with the help of impedance spectroscopy (Figure 3). The key feature of this sensor is that by forming the nanohybrid materials (RGO-NP hybrid) on the electrode, it results in an enhanced sensitivity toward CRP detection. The linear range of the sensor is 1–1000 ng/mL with an LOD of 0.08 ng/mL in serum samples. Based on the findings, it has the feasibility to employ multiplexed assay detection of biomarkers for point-of-care applications.

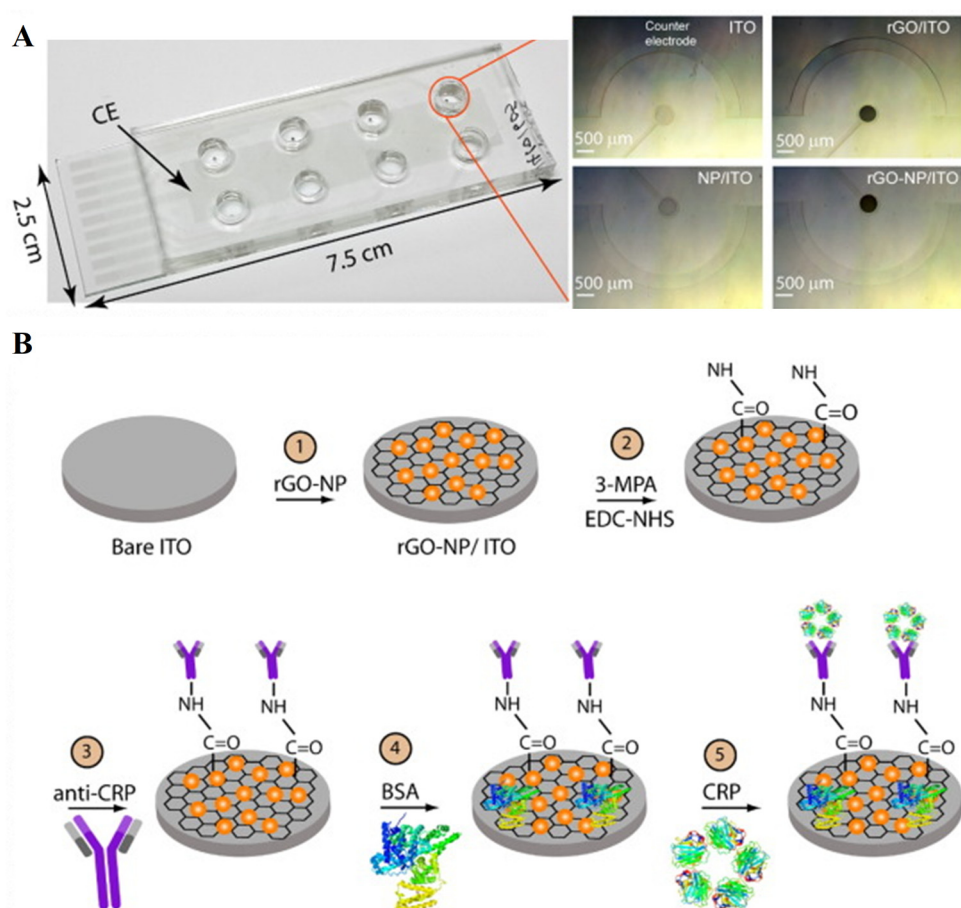


Figure 3. (A) Fabrication of 8-channel Indium-tin oxide electrodeposited with reduced graphene oxide-nanoparticle microdisk electrode array as working electrodes with a shared counter electrode. (B) Chemical functionalization of modified ITO electrode with EDC/NHS to couple antibodies for CRP detection in real samples. Reprinted with permission from Ref. [36]. Copyright 2016, Elsevier.

Jonous et al. [37] reported on the detection of prostate-specific antigen (PSA) by using a sandwich-type transducer composed of graphene oxide (GO) and gold nanoparticles (AuNPs). In this work the authors utilized an 11-mercaptopundecanoic acid for self-assembled monolayer formation on the GO-coated glassy carbon electrode (GCE) and a subsequent modification with EDC/NHS to convert -COOH to -NH for antibody bindings (Figure 4). After blocking with 1% BSA, different concentrations of PSA were allowed

to bind to the electrode and with square wave voltammetry, and the quantification was made. The sensor possessed a limit of detection estimated to be around 0.2 and 0.07 ng/mL for total and free PSA antigens, respectively. The incorporation of AuNPs on GO/GCE enabled double functionality, i.e., specific recognition and signal amplification, for sensitive determination of PSA.

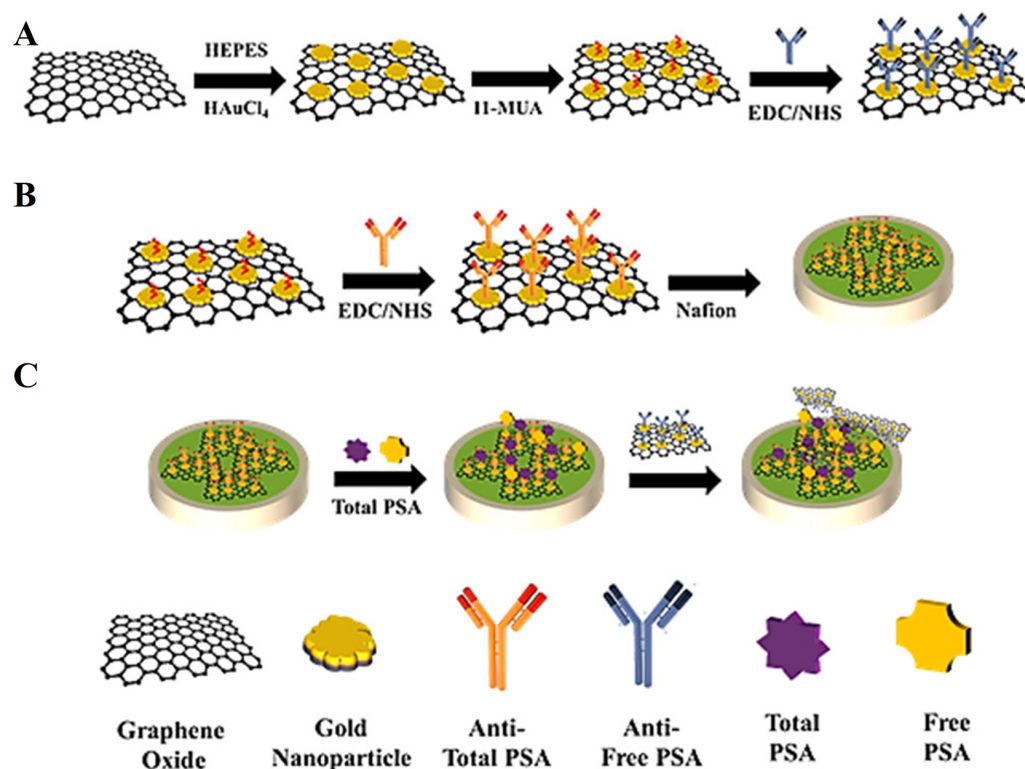


Figure 4. (A) Procedures for the fabrication of Go/GNP/Ab. (B) Procedure for preparing the electrochemical sensor. (C) Schematic illustration of the novel electrochemical sensor for PSA marker detection. Reprinted with permission from Ref. [37]. Copyright 2019, Wiley.

Also, Kasturi et al. [38] reported on the development of a biosensor for the detection of microRNA-122 (miRNA-122) with AuNPs-decorated reduced graphene oxide (rGO) on the Au electrode surface (Figure 5). The thiol-labeled DNA probes were attached to the Au-rGO transducer surface by forming a SAM layer, with subsequent blocking with 1% BSA. Then, the target miRNA was allowed to bind to the transducer surface to quantify the biomarker for liver diseases.

The sensor possessed a linear range from 10 μ M to 10 pM and had a detection limit of 1.73 pM. The sensor possessed good biocompatibility, superior electron transfer characteristics, large surface area, and selective conjugation with biomarkers. Also, the sensor design can be applied to construct other types of biomarker detection. Furthermore, it can be integrated with a lab on a chip platform. It is also applicable to the large-scale production of sensors with a focus on the early detection of diseases.

In another interesting work, Rauf et al. [39] reported on the use of laser-induced graphene oxide [34] as a new-generation electrode in cancer research for the detection of human epidermal growth factor receptor 2 (HER-2). In this study, with laser printing technology, the structures of working, counter, and reference electrodes were formed on a polyimide sheet, then the gold nanostructures (Christmas-tree-like structures) were formed by electrodeposition on the working electrode (Figure 6). Subsequently, the sensor surface is modified with thiol labeled HER-2 aptamer and blocked with BSA for any nonspecific bindings. Then, the HER-2 protein was allowed, in different concentrations, to interact with the aptamer immobilized surface. The electrochemical signals were then recorded for the aptamer surface after bindings with different concentrations with $[\text{Fe}(\text{CN})_6]^{3-/4-}$

redox probe. The CV analysis showed a decrease in current upon bindings of various concentrations of HER-2, and from the calibration, the limit of detection was found to be 0.008 ng/mL. It is claimed that with the incorporation of 3D Au nanostructures the sensor possessed a high electron transfer rate, which resulted in achieving a lower LOD and possessing high sensitivity and accuracy in detecting HER-2 in human serum samples. Furthermore, special software was developed to make it a POC device, in which the laboratory aptasensor could be converted into a hand-held aptasensor.

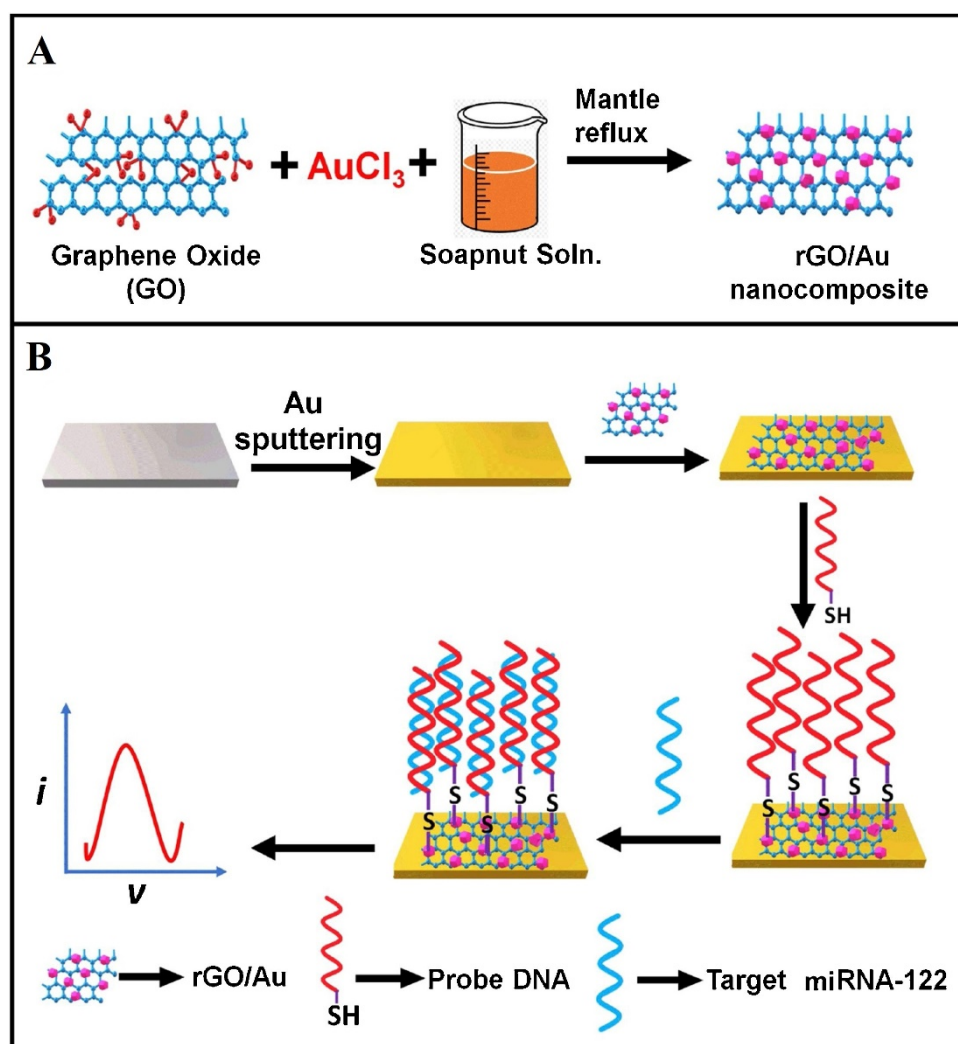


Figure 5. Schematic representation of the (A) Synthesis of rGO/Au nanocomposite, (B) Fabrication of rGO/Au nanocomposite-based miRNA-122 electrochemical detection platform. Reprinted with permission from Ref. [38]. Copyright 2021, Elsevier.

Also, Hasanjani et al. [40] reported on the development of Zidovudine (ZDV). A modified pencil graphite electrode (PGE) was made using deoxyribonucleic acid/Au-Pt bimetallic nanoparticles/graphene oxide-chitosan (DNA/Au-Pt BNP/GO-chit/PGE) (Figure 7). The PGE was immersed in the GO-chit solution to create the graphene oxide-chitosan/pencil graphite electrode (GO-chit/PGE). Later, the electrodeposition of Au-Pt bimetallic nanoparticles (Au-Pt BNP) was accomplished on the surface of the GO-chit/PGE-modified electrode. Subsequently, DNA was immobilized on the Au-Pt BNP/GO-chit/PGE, applying a constant potential of 0.5 V.

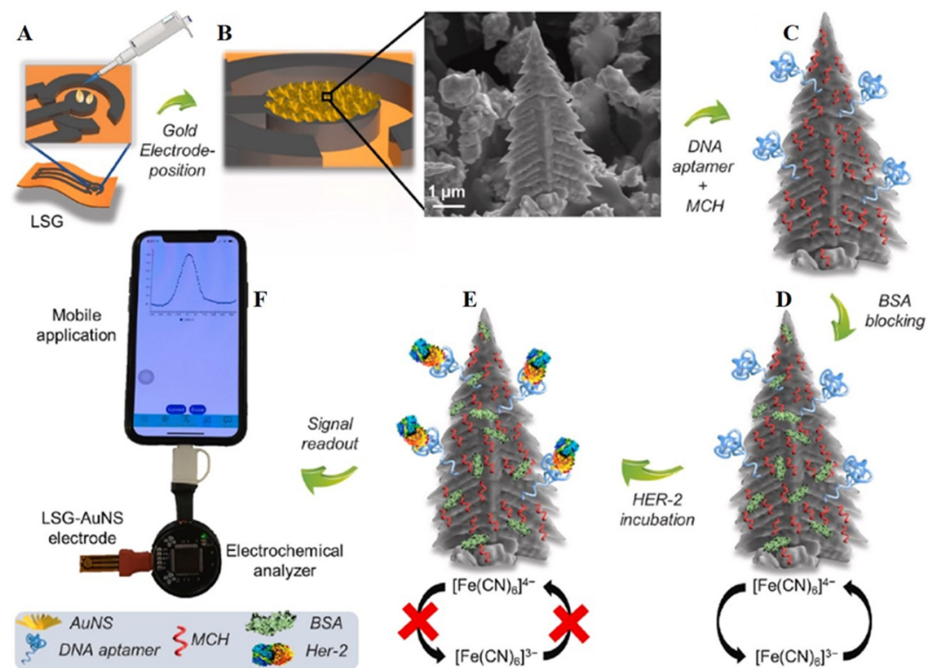


Figure 6. The schematic diagram for the formation of laser-induced graphene (LIG) electrode sensor. (A) LIG electrode on polyimide sheet, (B) Formation of Au nanostructures on working electrode area with electrodeposition, inset shows the SEM images of the tree-like structure of Au. (C) Bindings of DNA aptamer on the electrode through self-assembly of mercaptohexanol (MCH), (D) Surface blocking procedures with BSA and measurement of electrochemical signal with $[Fe(CN)_6]^{3-}/4^-$ redox probe, (E) Incubation with the HER-2 antigen and measurement of EC signal, and (F) Quantification of HER-2 by evaluating the electrochemical signal. Reprinted with permission from Ref. [39]. Copyright 2021, Elsevier.

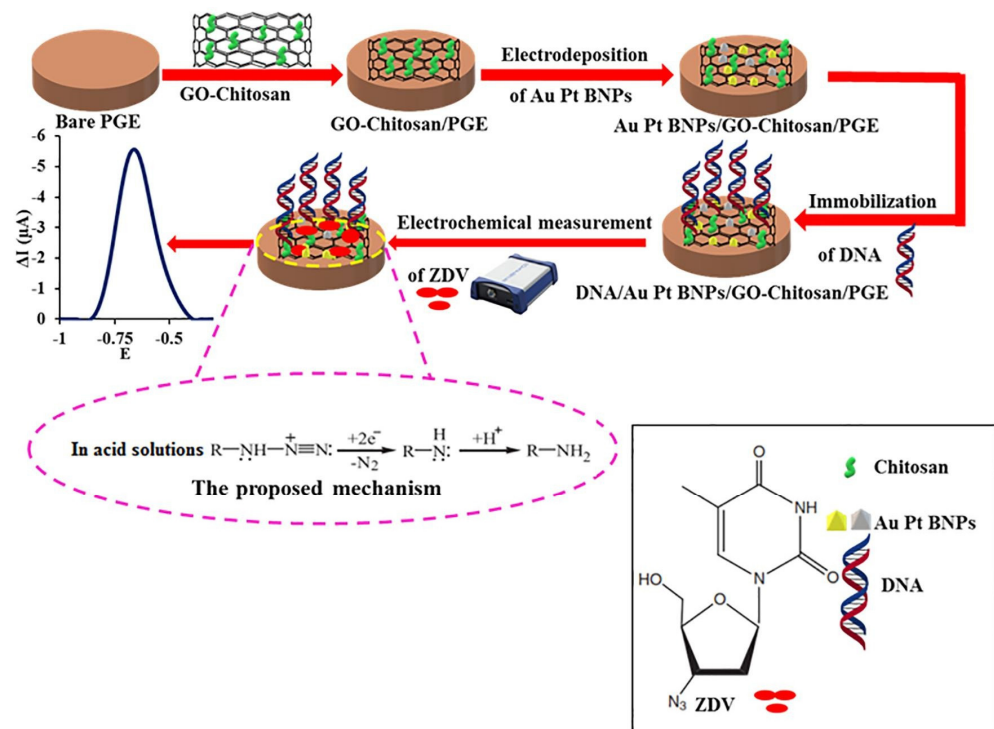


Figure 7. Schematic route for the fabrication of DNA/Au–Pt BNPs/GO–chit/PGE transducer surface for the development of an electrochemical biosensor for the detection of ZDV. Reprinted with permission from Ref. [40]. Copyright 2021, Elsevier.

Using differential pulse voltammetry, the I–V response was recorded for different concentrations of ZDV. The sensor showed a linear dynamic range from 0.01 pM to 10.0 nM, with a detection limit of 0.003 pM in human serum samples.

Recently, Kangavalli and Veerapandian reported on the development of a dengue biomarker using ruthenium bipyridine complex on the surface of graphene oxide [41]. They also reported on various EC-based techniques for the electrodeposition and electroless deposition procedures of graphene oxide as a nanoarchitecture for a label-free biosensor platform [42]. Some more information on electrochemical biosensors developed for biomarker detection that contain graphene oxide and metal nanoparticles can be found in some valuable studies recently reported, and are available in the literature [43–47]. Graphene oxide-based nanomaterials offer a wide range of possibilities for developing sensitive electrochemical biosensors for biomarker detection. In recent years, significant advances in graphene-nanoparticle-based electrochemical sensors are made for the detection of cancer biomarkers, and here we analyze the analytical parameters of those sensors, as shown in Table 1.

Table 1. Literature reports on the analytical parameters of graphene oxide conjugated nanoparticles for various biomarker detection.

Sensing Platform	Biomarker	Technique	Linear Range	LOD	Real Sample	Ref.
RGO-NP/ITO	CRP	EIS	1–10,000 ng/mL	0.08 ng/mL	Human serum	[36]
GO-CoPP	CPEB4	DPV	0.1 pg/mL–10 ng/mL	0.074 pg/mL	Human serum	[48]
AuNP-RGO/ITO	TNF- α	EIS	1–1000 pg/mL	0.43 pg/mL	Human serum	[49]
rGO@AgNPs	LA	CV	10–250 μ M	0.726 μ M	Human serum	[50]
AgPdNPs/rGO	RAC	LSA	0.01–100 ng/mL	1.52 pg/mL	—	[51]
	SAL			1.44 pg/mL		
	CLB			1.38 pg/mL		
MWCNTs-AuNPs/CS-AuNPs/rGO-AuNPs	OTC	DPV	1.00–540 nM	30 pM	—	[52]
GO-Fe ₃ O ₄ - β -CD	MGMT	DPV	0.001–1000 nM	0.0825 pM	Human plasma	[53]
AuNPs/GQDs/GO/SPCE	miRNA-21	SWV	0.001–1000 pM	0.04 fM	Human serum	[54]
	miRNA-155			0.33 fM		
	miRNA210			0.28 fM		
rGO/RhNPs/GE	HER-2-ECD	DPV	10–500 ng/mL	0.667 ng/mL	Human serum	[55]
AuNPs-rGO/ITO	IL8	DPV	500 fg/mL–4 ng/mL	72.73 pg/mL	—	[56]
Pd@Au@Pt/rGO	CEA	DPV	12 pg/mL–85 ng/mL	8 pg/mL	Human serum	[57]
	PSA		3 pg/mL–60 ng/mL	2 pg/mL		
AgNPs/GO/SPCE	PSA	DPV	0.75–100 ng/mL	0.27 ng/mL	Human serum	[58]
rGO-GNPs-Cr.6/GCE	L-Trp	SWV	0.1–2.5 μ M	0.48 μ M	Human serum	[59]
GO/AgNPs/Au	PSA	LSV	5–20,000 pg/mL	0.33 pg/mL	Human serum	[60]
AuNP/RGO/GCE	CA125	SWV	0.0001–300 U/mL	0.000042 U/mL	Human serum	[61]
ErGO-SWCNT/AuNPs	HER2	EIS	0.1 pg/mL–1 ng/mL	50 fg/mL	Human serum	[62]
Au-PtBNPs/CGO/FTO	MUC1	DPV	1 fM–100 nM	0.79 fM	Human serum	[63]
BNPAu-Fe-rGO/GCE	Acetaminophen	DPV	50–800 nM	0.14 nM	Human urine	[64]

2.2. MoS₂ Conjugated Nanoparticles for Electrochemical Biomarker Detection

Recently, transition metal dichalcogenides (TMDCs) found their applications in various biosensors due to their large surface-to-volume ratio, tunable electronic and optical properties, low toxicity, and unique van der Waals layered structure [65]. In TMDCs, one layer of transition metal atoms (M) lies between two layers of chalcogen atoms (X) resulting in a formula MX₂. Various kinds of TMDCs can be realized by altering the chalcogen atoms such as Sulphur (S), Selenium (Se), and Tellurium (Te), and metal atoms like Molybdenum (Mo) and Tungsten (W). Among these, MoS₂ is commonly used because its fundamental constituents are surplus and innocuous [66]. MoS₂ molybdenum (Mo) atoms lie between the two sulfide atoms layers (S-Mo-S) and atoms in the crystal are associated by strong

covalent bonding and adjacent layers of MoS₂ are held by weak van der Waals forces. MoS₂ possesses a mobility of 200 cm²/Vs at room temperature, high on/off current ratio of 10⁸, and a direct band gap of 1.8 eV. Based on these properties, MoS₂ becomes a promising alternative to graphene and is applied in various electrochemical and optical sensors [67–69]. MoS₂ can be synthesized in both top-down and bottom-up approaches (Figure 8). The top-down approach includes the exfoliation of MoS₂ [70], while the bottom-up approaches include (i) chemical vapor deposition [71]; (ii) physical vapor deposition [72]; (iii) solution-based processing [73]. For a more detailed synthesis of MoS₂, readers are encouraged to go through the literature survey of the desired synthesis approach. Thus, like graphene, MoS₂ offers a large surface area that enhances its biosensing performance.

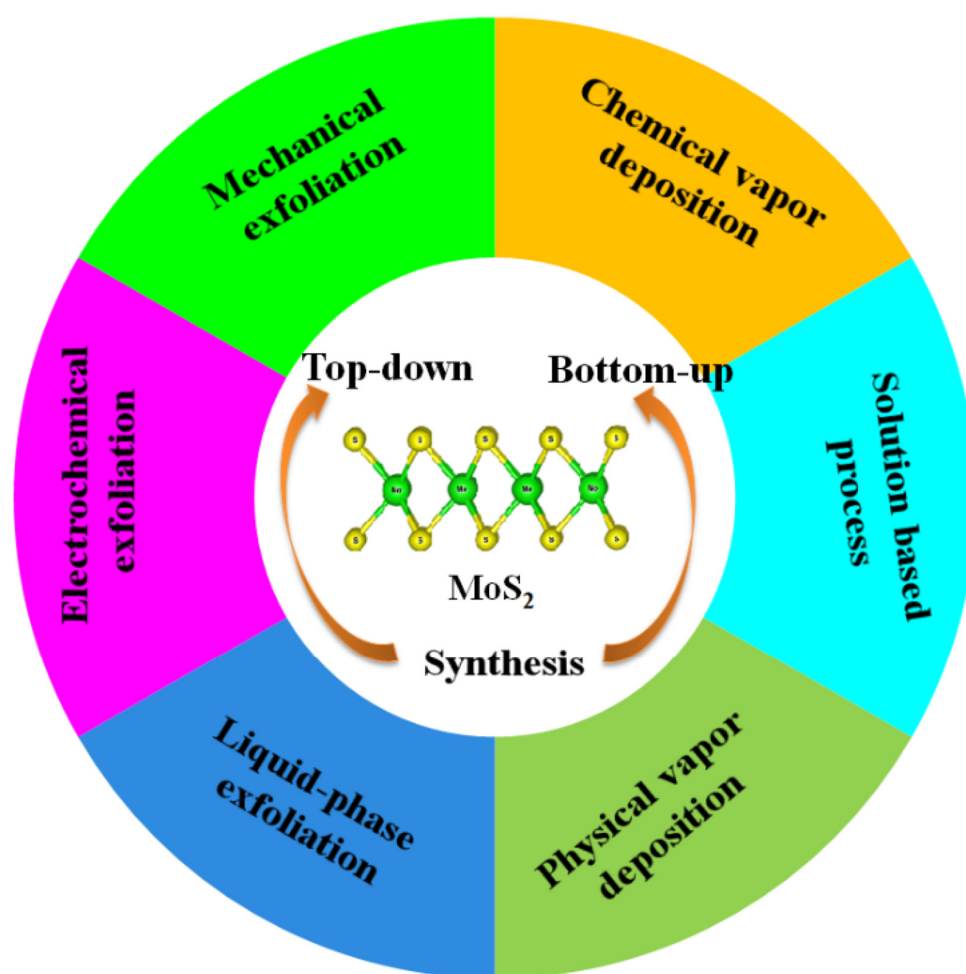


Figure 8. Various synthetic methods for MoS₂ preparation. Reprinted with permission for Ref. [74]. Copyright 2022 MDPI.

MoS₂ possesses a direct band gap of 1.8 eV in the monolayer, lattice defects of zero dimensionality, grain boundary defects, and an enhanced surface-to-volume ratio. Also, the feasibility of surface modification and chemical functionalization makes these characteristics of MoS₂ to adopt and study in scientific and industrial fields [75] (Figure 9). Furthermore, to increase the electroactivity/conductivity of graphene and/or other 2D materials, mostly nanoparticles were incorporated to achieve the synergistic effects from both nanomaterials, which ultimately resulted in an improvement in the overall analytical performance of the biosensor. In this section, we review various types of biosensors that incorporate metal nanoparticles on MoS₂ for the detection of various biomarkers.

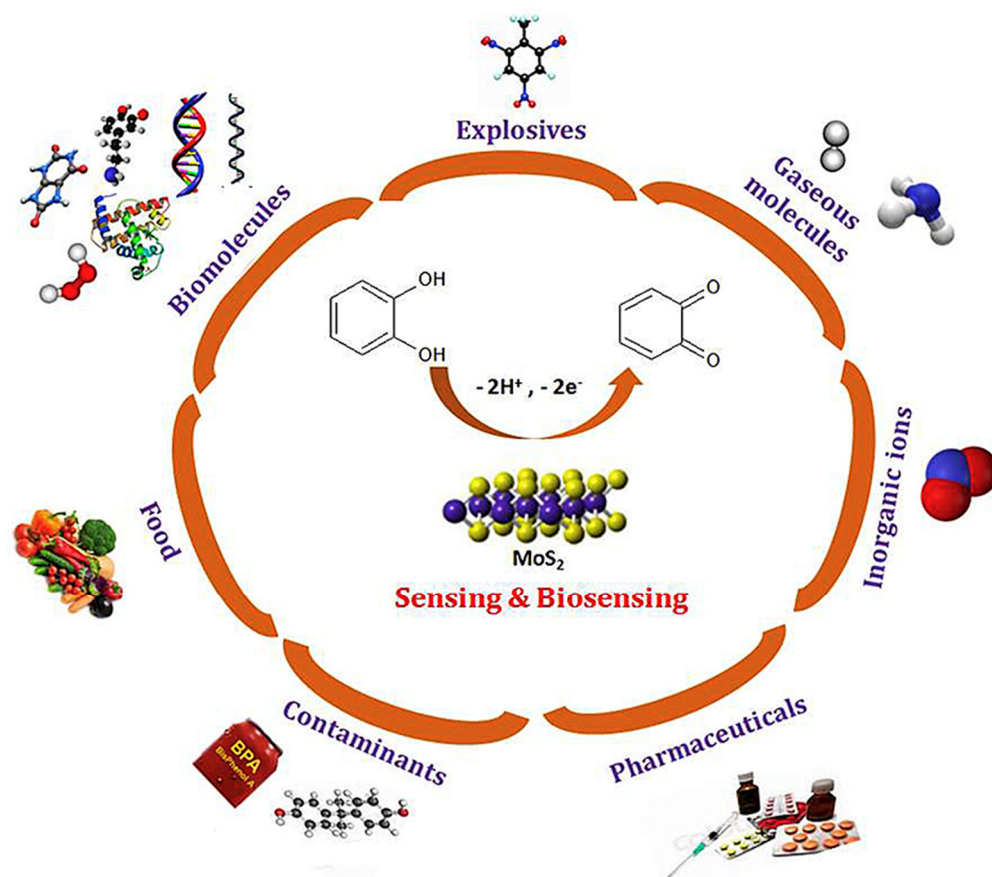


Figure 9. MoS₂ nanostructures-based electrochemical sensing application in various fields. Reprinted with permission from Ref. [76]. Copyright 2018, Elsevier.

In a recent report that mentions the usage of MoS₂-Au nanoparticles, Yagati et al. [77] reported on the applications of MoS₂ conjugated Au nanoparticles on indium tin oxide (ITO) electrodes for the detection of the thyroid-stimulating hormone biomarker, triiodothyronine (T₃), as shown in Figure 10. Electrodeposition procedures allowed the formation of MoS₂ and Au nanostructures on the ITO electrode. Subsequently, T₃ antibodies were immobilized on the MoS₂-Au/ITO surface by forming a self-assembled monolayer of dithiobis (succinimidyl propionate) (DSP). For any nonspecific bindings, the surface is coated with casein and then subjected to different concentrations of the T₃ biomarker diluted in both PBS and serum samples. Electrochemical impedance spectroscopy was used to analyze the bindings of T₃ to its antibodies and a linear correlation was observed for different concentrations. Based on the quantifications made by this sensor for the detection of T₃, a linear range of 0.01–100 ng/mL with a detection limit of 2.5 pg/mL was observed. The sensor also showed a good correlation with data observed by the conventional method (Roche Cobas) and possessed high sensitivity and selectivity in discriminating the healthy and cancer samples. Based on the findings, the developed sensor could apply to cancer-related biomolecule analysis.

Su et al. [78] developed dual target sensing (adenosine triphosphate (ATP) and thrombin) detection electrochemical biosensors based on gold nanoparticles-decorated MoS₂ (AuNPs–MoS₂) nanocomposites which feature both “signal-on” and “signal-off” elements in the detection system, and thrombin and ATP could act as inputs to activate an AND logic gate (Figure 11). In this approach, two different aptamer probes labeled with redox tags (ferrocene (Fc) and methylene blue (MB)) were simultaneously immobilized on an AuNPs–MoS₂ modified glassy carbon electrode (GCE) through Au–S bond formations. Subsequently, the electrode was immersed in 6-mercaptohexanol to block the uncovered spots of AuNPs–MoS₂/GCE. Square wave voltammetry (SWV) was used to determine the

various concentrations of ATP and thrombin applied to the GCE. From concentration vs. change in the current results, it was evaluated that the sensor had a linear range for the determination of ATP, which was 1 nM to 10 mM with a detection limit of 0.32 nM, while for the thrombin determination, the linear range was 0.01 nM to 10 μ M with a detection limit of 0.0014 nM.

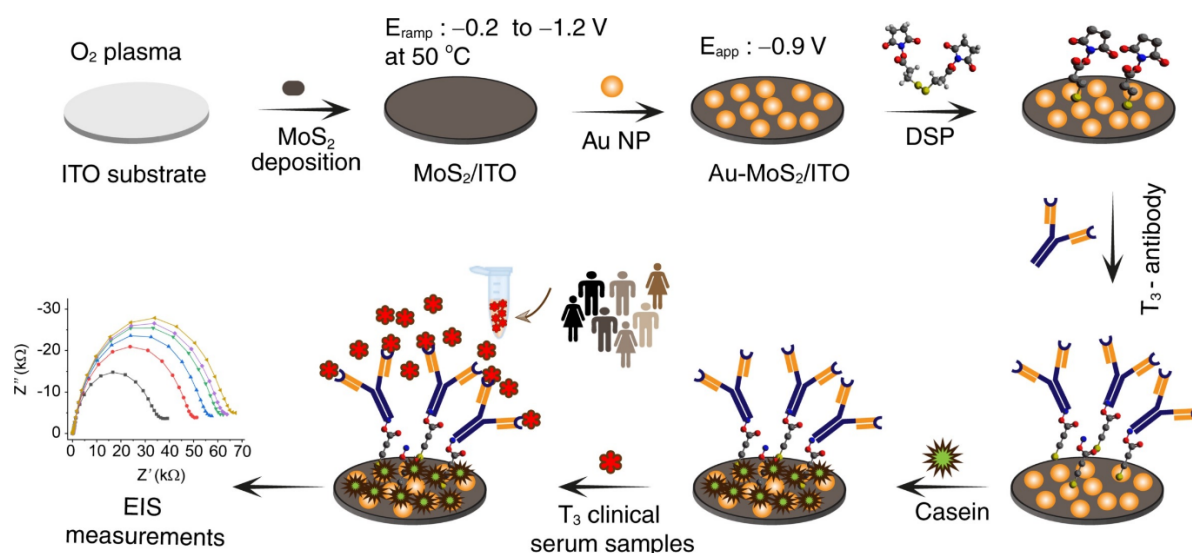


Figure 10. Schematic illustration of the total triiodothyronine (T_3) receptive interface fabrication through the immobilization of the antibody on a step-by-step modification process of MoS_2 -Au formation and subsequent functionalization with a dithiobis (succinimidyl propionate) monolayer on an indium tin oxide electrode surface. With increasing concentration of the T_3 analyte in serum, the EIS (Nyquist plot) shows increased semi-circle (R_{ct}) for quantification. Reprinted with permission from Ref. [77]. Copyright 2020, Elsevier.

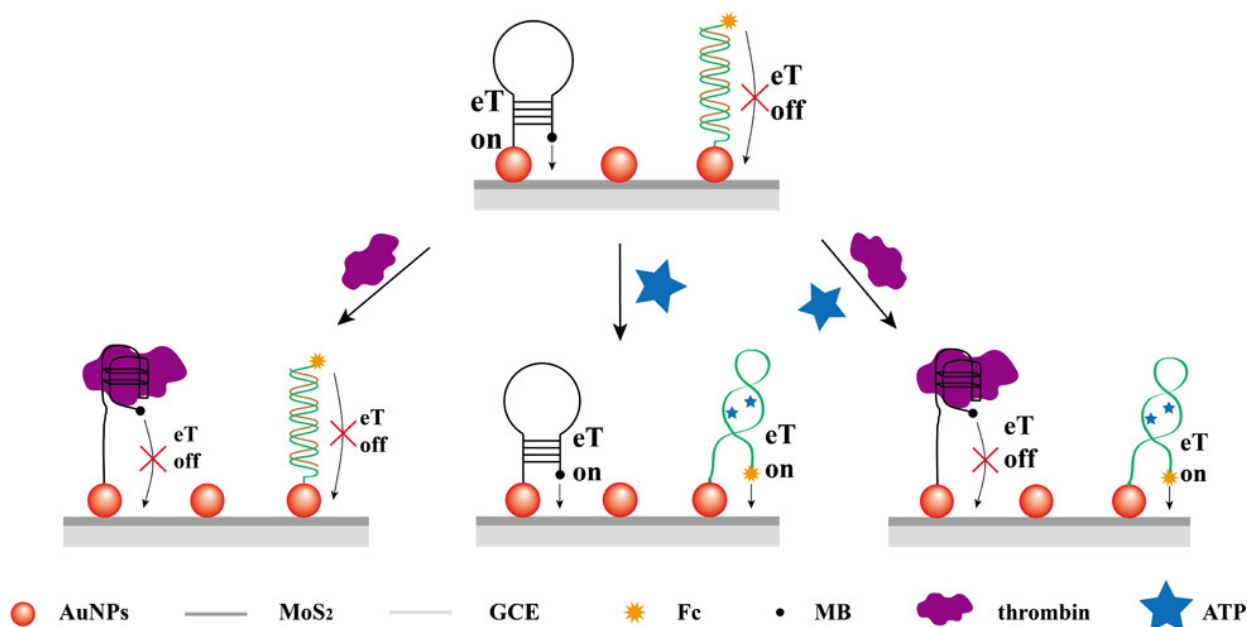


Figure 11. Schematic representation for the development of the aptasensor for the determination of ATP and thrombin. Reprinted with permission from Ref. [78]. Copyright 2016, ACS.

The authors also suggested that this mechanism can be acted as an AND logic gate by using ATP and thrombin as inputs and the electrochemical signals of Fc and MB as outputs (Figure 12). The logic gate works on the structural conversion of the aptamer probe

triggered by ATP and thrombin. The working mechanism was the individual peak current enhancement of Fc or the suppression of MB as electron transfer OFF (eTOFF) or “zero” output, and the simultaneous peak current enhancement of Fc and suppression of MB as electron transfer ON (ON) or “one” output. From the inset table, a “one” output was achieved only when both inputs were “one”. When there were no inputs (0, 0) or only one input (0, 1 or 1, 0), the result was “zero” output. Thus, the MoS₂-based multiplexed aptasensor could also serve as an “AND” gate.

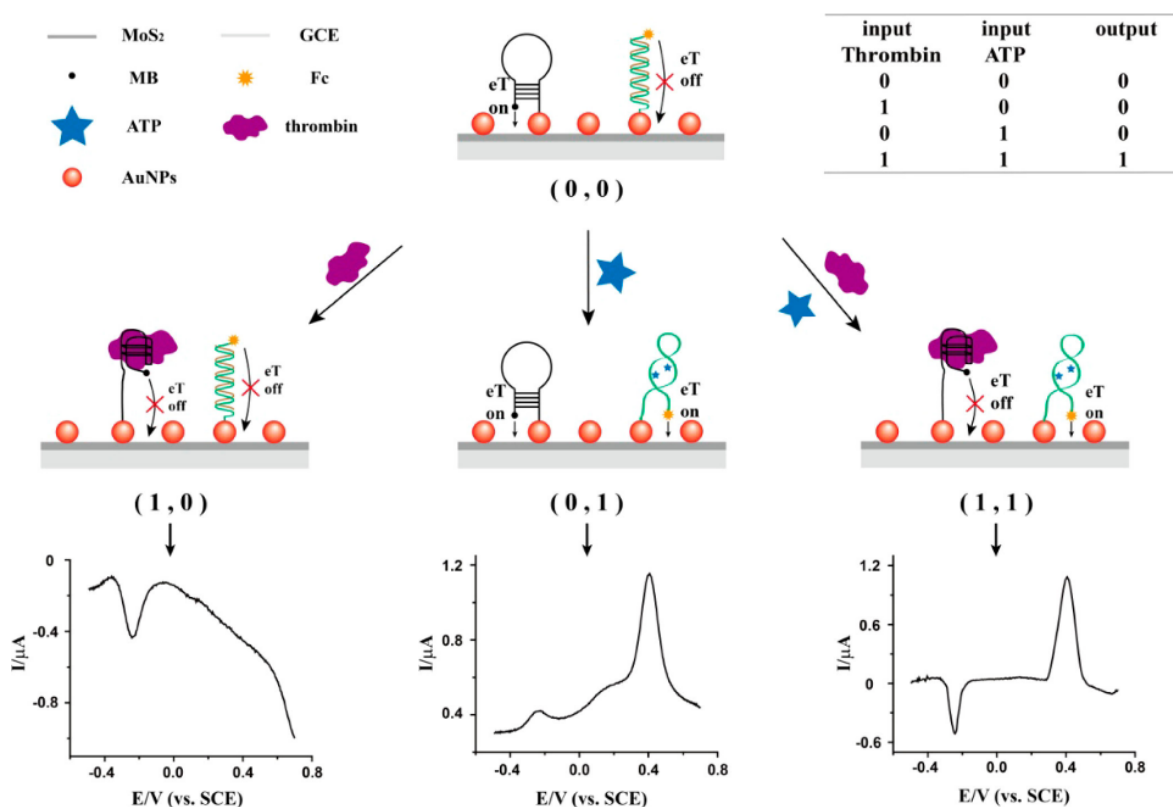


Figure 12. Schematic description of the MoS₂-Based AND logic gate for determination of ATP and thrombin. Reprinted with permission from Ref. [78]. Copyright 2016, ACS.

In another work, Chen et al. [79] reported on the development of a growth differentiation factor-15 (GDF-15) expression sensor which is a potential biomarker for the diagnosis, risk stratification, and prognosis of various cardiovascular diseases (Figure 13). Here, a sandwich-type immunosensor was constructed using amine-modified graphene-supported gold nanorods (NG/AuNPs) as a substrate platform, and the durian-shaped MoS₂/AuPtPd nanodendrite (NDs) as a label for secondary antibodies (Ab₂) for the quantification of growth differentiation factor-15 (GDF-15). NG/AuNPs are used to enhance the surface area and for the immobilization of primary antibodies through the binding of amino or sulfhydryl groups. Subsequently, the electrodes were blocked with 1wt% BSA. Finally, the signal probe MoS₂/AuPtPd-Ab₂ was added to the sample.

The developed sensor was also applied to evaluate the efficacy towards the clinical sample analysis and compared with traditional sensing methods, such as ELISA, to evaluate the accuracy of the results. The sensor showed a linear range of 1.5 pg/mL to 1.5 μg/mL with a detection limit of 0.9 pg/mL. Due to its high sensitivity, rapid response, and feasibility to miniaturization, the proposed sensor could be applied to a point-of-care diagnostic tool for cardiovascular diseases and paves the path toward “liquid biopsies”.

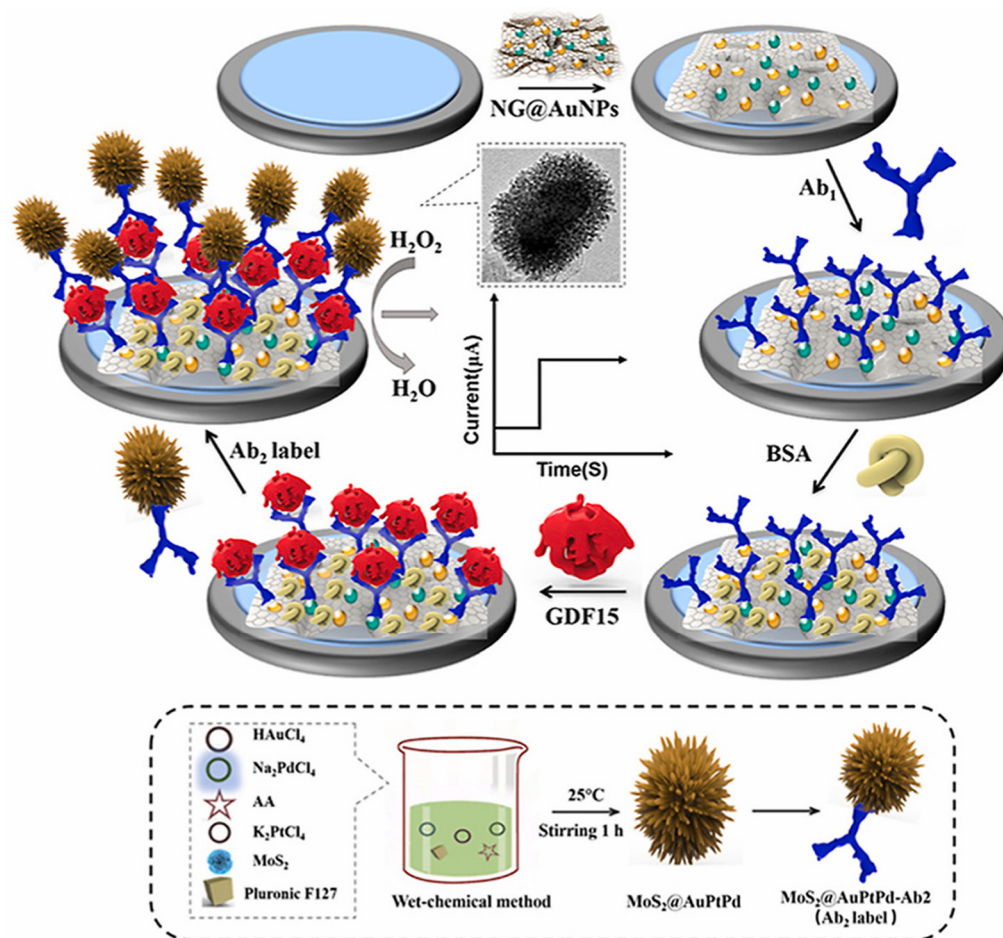


Figure 13. Schematic illustration for the development of a sandwich-type electrochemical sensor for GDF-15 detection sensor. Reprinted with permission from Ref. [79]. Copyright 2022, Elsevier.

Nong et al. [80] reported on the detection of cortisol which is a glucocorticoid hormone that adrenal glands produce and release, and this hormone regulates stress, inflammation, blood pressure, sugar, and overall metabolism. In this work, copper tungstate-molybdenum sulfide ($\text{CuWO}_4@MoS_2$) and chitosan-gold (Chit-Au) nanocomposite were synthesized and applied to GCE (Figure 14). Subsequently, the cortisol antibody (C-Mab) was immobilized using the EDC/NHS reaction and subsequent blocking with BSA. Once the transducer surface was fabricated, SWV was performed to analyze the bindings of various concentrations of cortisol and a linear relationship was observed concerning different concentrations. The sensor showed a linear range of 0.1 fg/mL to 1 $\mu\text{g/mL}$ with a detection limit of 0.014 fg/mL ($S/N = 3$). The sensor showed excellent storage stability and reproducibility and it can detect the content of cortisol in saliva.

Su et al. [81] reported on the use of a MoS_2 -Au nanocomposite for the detection of a carcinoembryonic antigen (CEA). In this work, CEA antibodies labeled with horseradish peroxidase resulted in an amplified electrochemical signal by catalyzing o-phenylenediamine (o-PD) in the presence of hydrogen peroxide (H_2O_2). As can be seen in Figure 15, the MoS_2 -Au conjugated HRP labeled antibodies enhance the overall sensitivity when the different concentrations of CEA were measured using cyclic voltammetry. From the analytical performance, the sensor displayed a linear range of 10 fg/mL to 1 ng/mL with a detection limit of 1.2 fg/mL. The sensor also exhibited good stability, and high selectivity suggesting that the proposed immunosensor could detect CEA in real samples.

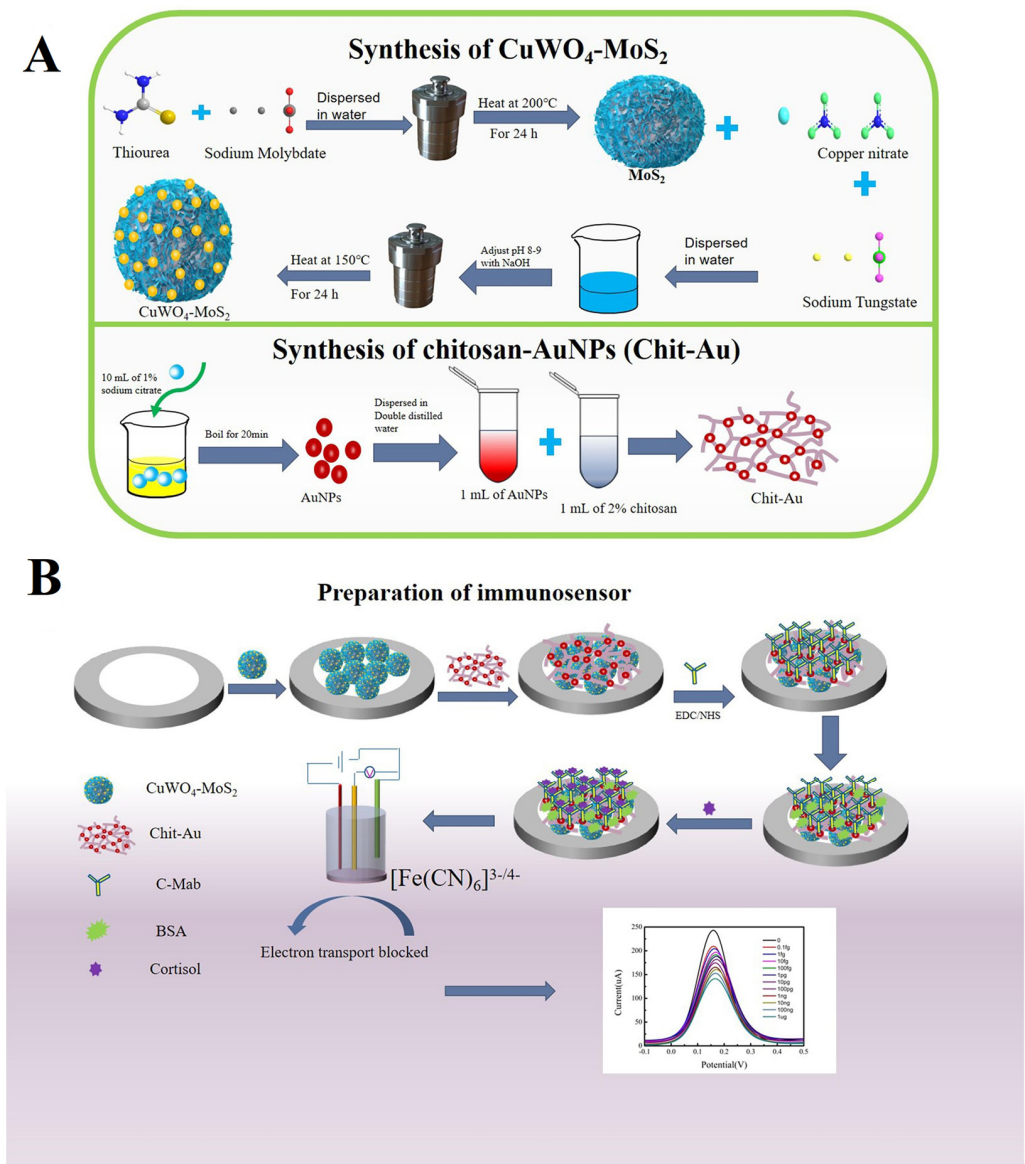


Figure 14. Schematic representation for (A) Synthesis of MoS_2 , $\text{CuWO}_4\text{@MoS}_2$, AuNPs, and Chit-Au nanocomposites; (B) Preparation process of the immune electrode. Reprinted with permission for Ref. [80]. Copyright 2022, Elsevier.

Also, Ma et al. [82] reported similar works using $\text{MoS}_2\text{@Cu}_2\text{O-Au}$ nanoparticles for the detection of alpha-fetoprotein (AFP), a tumor marker to identify adult primary liver cancer (Figure 16). In this work, AuNPs were electrodeposited on GCE which acted as antibody carriers and sensing platforms. Further, $\text{MoS}_2\text{@Cu}_2\text{O}$ was combined with the AuNPs as a strategy to obtain the signal amplification resulting in a composite $\text{MoS}_2\text{-Cu}_2\text{O-Au}$ as a triamplification electrochemical signal. A sandwich immunosensor was developed by immobilizing primary antibodies on Au-deposited GCE and blocked with a surface with BSA for nonspecific bindings. Then, the electrodes were dipped with different concentrations of AFP. Subsequently, the HRP-labeled secondary antibodies coupled with $\text{MoS}_2\text{@Cu}_2\text{O}$ were then allowed to conjugate with the electrode. Amperometric response, under suitable experimental conditions, exhibited that the sensor possessed a linear range of 0.1 pg/mL to 50 ng/mL and a detection limit of 0.037 pg/mL ($S/N = 3$). The sensor showed satisfactory recoveries when tested in human serum samples, and the proposed approach could extend the potential application of electrochemical immunosensors to medical applications.

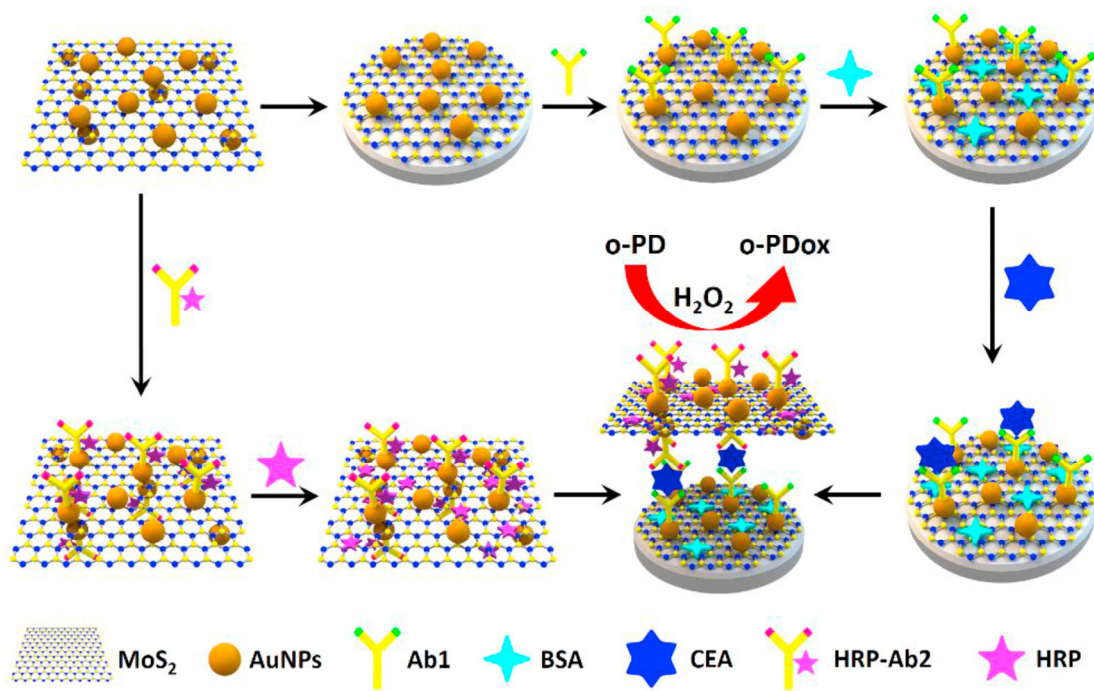


Figure 15. The schematic diagram for the stepwise modification of the GCE with MoS₂ and Au nanoparticles for anti-CEA antibody immobilization for developing a CEA detection sensor. Reprinted with permission from Ref. [81]. Copyright 2019, Elsevier.

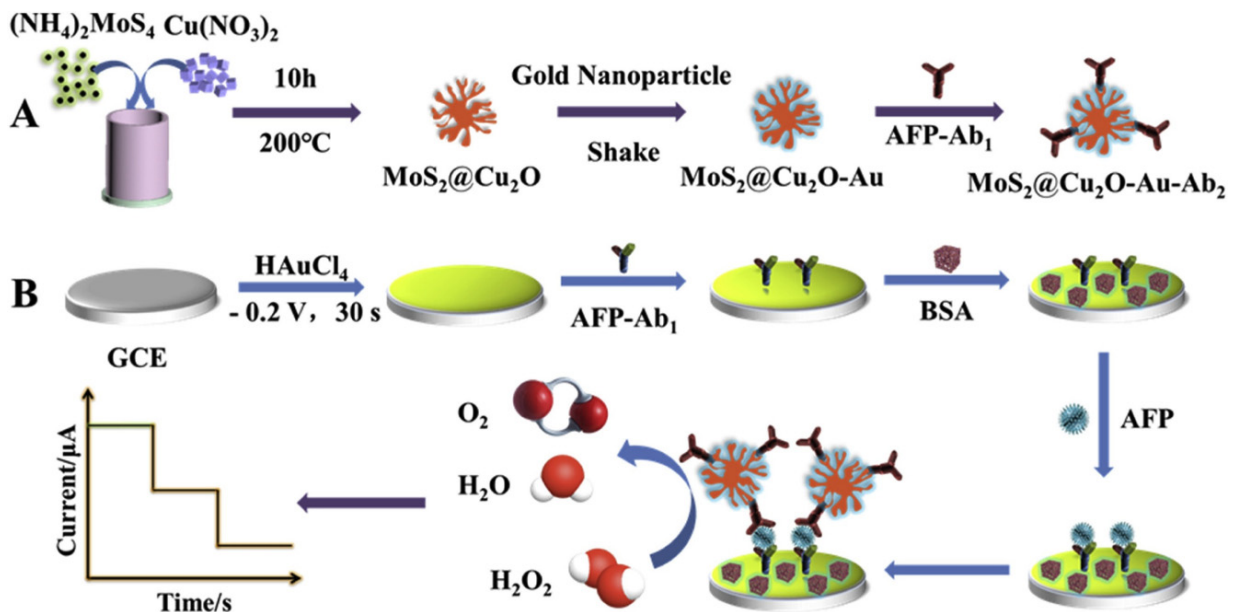


Figure 16. The schematic diagram for the preparation procedure for the sandwich-type electrochemical immunosensor. Reprinted with permission from Ref. [82]. Copyright 2019, Elsevier.

Likewise, several reports demonstrated the usage of a MoS₂-Au nanocomposite for the detection of electrochemical biosensors for various types of biomarker detection in clinical applications. However, very few reports show the possibility of point-of-care applications. Here, we analyzed the analytical parameters of the reports that adopt the MoS₂-Au nanocomposite used for electrochemical sensors and presented them in the following Table 2.

Table 2. Literature reports on the analytical parameters of MoS₂ conjugated nanoparticles for various biomarker detections.

Sensing Platform	Biomarker	Technique	Linear Range	LOD	Real Sample	Ref.
Au-NPs/MoS ₂	CRP	EIS	1 fg/mL–1 µg/mL	0.01 fg/mL	—	[83]
Fe ₃ O ₄ @MoS ₂ -AuNPs	H ₂ O ₂	SWV	1–120 µM	80 nM	Human serum	[84]
Au/MoS ₂ /Au/PET	GP120	SWV	0.1 pg/mL–10 ng/mL	0.066 pg/mL	Human serum	[85]
MoS ₂ /Pt@Au-nanoprism/PDA	free-PSA; total-PSA	DPV	0.0001–100 ng/mL	0.1 pg/mL; 0.0011 fg/mL	Human serum	[86]
MoS ₂ NFs/Au@AgPt YNCs	CEA	i-t curve	10 fg/mL–100 ng/mL	3.09 fg/mL	Human serum	[87]
Au/Co-BDC ^f /MoS ₂	CTnI ^f	i-t curve	10 fg/mL–100 ng/mL	3.02 fg/mL	Human serum	[88]
Au/MoS ₂ /rGO	CA 27-29 BCA	i-t curve	0.1–100 U/mL	0.08 U/mL	Human serum	[89]
MoS ₂ -AnNPs/GCE	CEA	DPV	1 pg/mL–50 ng/mL	0.27 pg/mL	Human serum	[90]
Ce-MoS ₂ /AgNRs	PSA	CV	0.1–1000 ng/mL	0.051 ng/mL	Human serum	[91]
MoS ₂ @Au	Siglec-5	ECL	10 pM–500 pM	8.9 pM	Human serum	[92]
MoS ₂ /PPY/AuNPs	Glucose	DPV	0.1–80 nM	0.08 nM	Human serum	[93]
AgPt/MoS ₂	H ₂ O ₂	i-t curve	20 µM–4 mM	1.0 µM	—	[94]

2.3. Biomarker Detection on MXenes Conjugated with Metal Nanoparticles

MXenes are transition-metal carbides/nitrides/carbonitrides with a 2D structure and general formula $M_{n+1}X_nT_x$ ($n = 1-3$), where M is an early transition metal, X can be carbon or nitrogen, and T_x corresponds to the surface terminations (Figure 17A,B). The ideal electronic structure [95], structural stability [96], high surface-to-volume ratios [97], outstanding mechanical [98] and optical properties [99], versatile surface chemistries [100], tunable bandgap [101], and high thermal and chemical stability [102,103] make them promising materials for biomarker detection (Table 3). The initial synthesis approach for MXenes was realized based on the etching of Ti_3AlC_2 with 50% HF for 2 h at room temperature [104]. Later many environmentally friendly approaches were formulated [105] (Figure 17C). However, similar to any other pristine 2D materials, MXenes suffer from poor selectivity, low sensitivity, and slow response [106]. These disadvantages were usually overcome by synthesizing MXene-metal nanoparticle nanocomposites. MXene-metal nanoparticle nanocomposites possess a large specific surface area, superior electron conductivity, and enhanced electron transfer properties for biosensing applications [107]. To expand beyond the limitations of MXenes, Liu et al. [108] reported the covalent grafting of PAMAM onto MXene (MXene@PAMAM) (Figure 18A). Here, the PAMAM acted as an efficient stabilizer and spacer, thereby preventing the restacking and oxidation of the MXene. Moreover, the aminoterminals of PAMAM acted as adsorption sites for AuNPs. The AuNPs@MXene@PAMAM nanobiosensing platform was applied for the detection of the cardiovascular disease biomarker cTnT. The sensor performance was remarkable with a wide detection range (0.1–1000 ng/mL) and a very low detection limit (0.069 ng/mL). Medetalibeyoglu et al. [109] fabricated a d- $Ti_3C_2T_x$ MXene@AuNPs/Ab2 bioconjugate-based sandwich-type electrochemical immunosensor for the detection of PSA. Here, AuNPs at the bioconjugate were used to label PSA secondary antibody-2 for signal amplification (Figure 18B). In one study, Laochai et al. [110] fabricated thread-based L-Cys/AuNPs/MXene working electrodes for the noninvasive electrochemical detection of sweat cortisol, which is an important biomarker for identifying adrenal gland disorders (Figure 18C). Here, MXene served as a 2D platform to anchor the monoclonal anticortisol antibodies, whereas AuNPs increased the specific surface area, and thereby the sensitivity of the detection system. Mesoporous nanoparticles (MNPs), comprising metallic and nonmetallic counterparts, show better catalytic performance compared to their bulk nanoparticles [111]. Liu et al. [112] reported sandwich-type PdPtBP MNPs/MXene-based immunosensor for the ultrasensitive detection of urine kidney injury molecule-1(KIM-1) (Figure 18D). Yang et al. [113] reported an interesting cascaded signal amplification strategy on in situ reduced gold nanoparticle deposited Ti_3C_2 MXene (Figure 18E), where MXene

acted as a stabilizer and reductant. Here, AuNPs with the predominant (111) facet on MXene provided high electrocatalytic activity and were also used as a carrier of the C-DNA and to make DNA hybridization. Mohsen et al. [114] reported Au nanoparticles on Ti_3C_2 MXene for synergistic signal amplification (Figure 18F). Here, the perfectly distributed Au nanoparticles on the flaky architecture of MXene contributed to the enhanced electrochemical performance and the attomolar detection of multiple micro-RNAs (miRNAs) achieved on an AuNP@MXene/Au electrode. Wang et al. [115] proposed a competitive electrochemical aptasensor for the breast cancer biomarker Mucin1 based on Au nanoparticles decorated Ti_3C_2 MXene. Here, aptamer binding to the electrode surface was achieved through Au-S bonds by the electrodeposited gold nanoparticles. The electrochemical aptasensor reported a wide linear range (1.0 pM–10 μM) and a low detection limit (0.33 pM) with promising clinical applications. Cheng et al. [116] demonstrated a gold nanoparticle-modified MXene-based sandwich-type immunosensor platform for squamous cell lung cancer cytokeratin fragment antigen 21-1 (CYFRA 21-1).

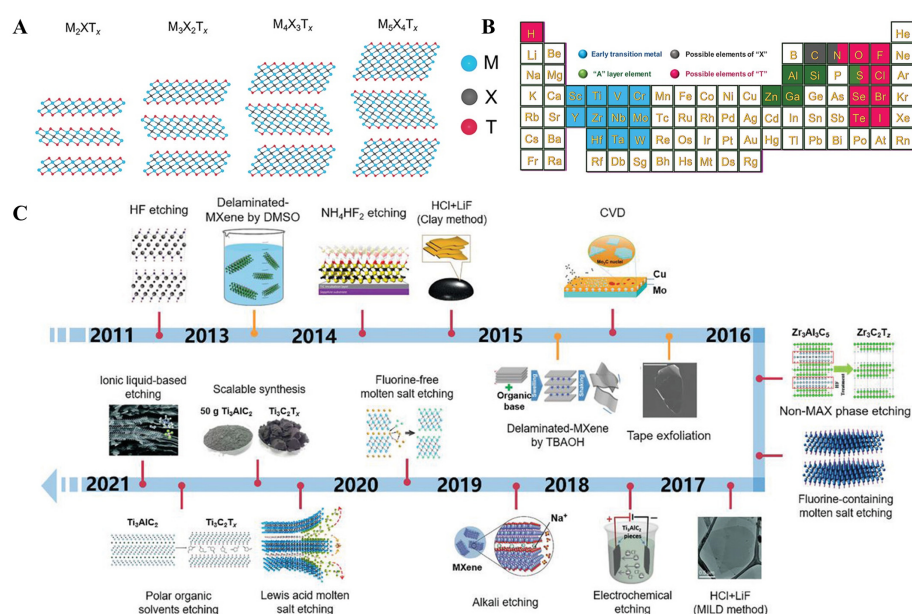


Figure 17. (A) Structure of various MXenes with surface terminations. (B) Periodic table elements experimentally used for the synthesis of MXenes, and (C) Timeline of the various synthesis routes to MXenes. Reproduced with permission from Ref. [117]. Copyright 2021, Wiley.

Table 3. Recent literature reports on metal nanoparticles incorporated MXenes for electrochemical biomarker detection.

Sensing Platform	Biomarker	Technique	Linear Range	LOD	Real Sample	Ref.
AuNPs/ Ti_3C_2 @PAMAM	cTnT	DPV	0.1–1000 ng/mL	0.069 ng/mL	Human serum	[108]
Ti_3C_2 @AuNPs	PSA	DPV	pg/mL	3.0 fg/mL	Plasma	[109]
L-cys/AuNP/ Ti_3C_2	Cortisol	CA	5–40 ng/mL	0.54 ng/mL	Artificial sweat	[110]
PdPtBP MNPs/ Ti_3C_2	KIM-1	DPV	0.5–100 ng/mL	86 pg/mL	Human urine	[112]
AuNPs- Ti_3C_2 /AuE	miRNA-21	DPV	100 aM–1 nM	50 aM	—	[113]
AuNP@MXene/Au	miRNA-21 miRNA-141	DPV	500 aM–50 nM	204 aM 138 aM	Total plasma	[114]
cDNA-Fc/MXene/Apt/Au/GCE	MUC1	SWV	0.001–1.0 $\times 10^4$ nM	0.33 $\times 10^{-3}$ nM	Human serum	[115]
AuNP- Ti_3C_2	CYFRA21-1	SWV	0.5–1.0 $\times 10^4$ pg/mL	0.1 pg/mL	Human serum	[116]
MCH/CP/MXene-Au/GCE	miRNA-377	SWV	10 aM–100 pM	1.35 aM	Human serum	[118]
Ti_3C_2 -AuNPs/GCE	PSA	DPV	1–50,000 pg/mL	0.31 pg/mL	—	[119]
AuNPs/d-S- Ti_3C_2	PCT	DPV	0.01–1.0	2.0 fg/mL	—	[120]
MB/DNA/HT/HP1/AuNPs/ Ti_3C_2 /BiVO ₄ /GCE	VEGF ₁₆₅	PEC	10 fM–100 nM	3.3 fM	—	[121]

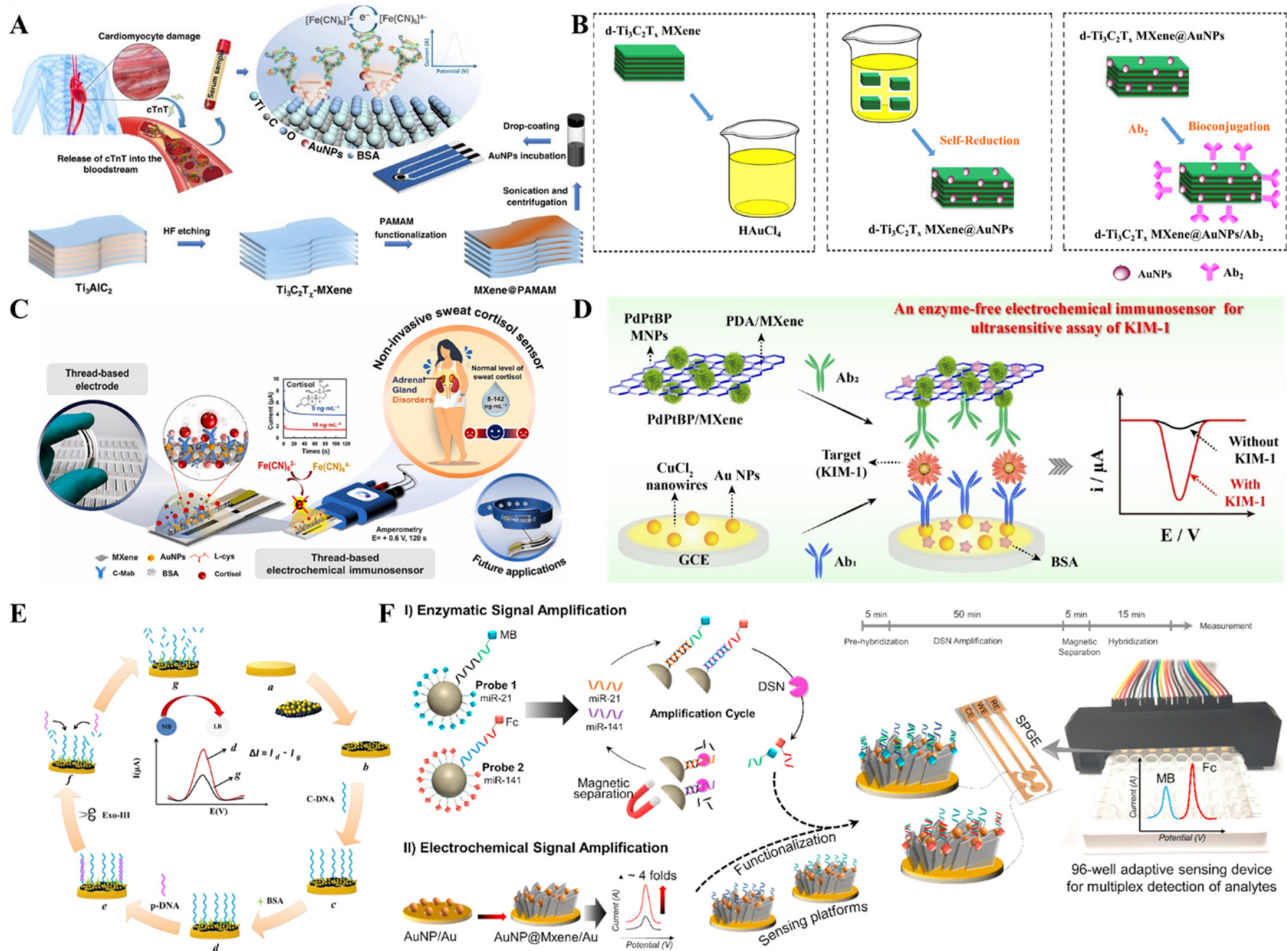


Figure 18. (A) Schematic illustration of the fabrication of AuNPs/MXene@PAMAM for the electrochemical detection of cTnT. Reproduced with permission from Ref. [108]. Copyright 2022, Nature. (B) Preparation of $d-Ti_3C_2$ MXene@AuNPs/Ab₂ for the detection of PSA. Reproduced with permission from Ref. [109]. Copyright 2020, Elsevier. (C) Fabrication of L-cys/AuNPs/MXene on a thread-based electrochemical biosensor for noninvasive sweat cortisol detection. Reproduced with permission from Ref. [110]. Copyright 2022, Elsevier. (D) Fabrication of PdPtBP nanoparticles/MXene-based enzyme-free electrochemical biosensor for the detection of kidney injury molecule-1 (KIM-1). Reproduced with permission from Ref. [111]. Copyright 2021, Elsevier. (E) Schematics of the AuNPs-based cascaded signal amplification process for the detection of miRNA-21. Reproduced with permission from Ref. [113]. Copyright 2022, ECS, and (F) Schematic diagram based on AuNPs decorated MXene for the multiplex and concurrent detection of miR-21 and miR-141. Reproduced with permission from Ref. [114]. Copyright 2020, Elsevier.

2.4. MOFs Conjugated Metal Nanoparticles for Electrochemical Biomarker Detection

As an emerging material with exceptional properties, metal-organic frameworks (MOFs) have been studied exceptionally during the past decades. MOFs are porous materials comprising a framework of metal ions or metal-containing clusters and organic ligands [122]. MOFs have been reported to have excellent properties such as a tunable structure [123], large surface area [124], abundant functional groups [125], high porosity [126], good conductivity [127], and thermal stability [128]. MOFs have been traditionally synthesized by hydrothermal/solvothermal methods [129]. The solvothermal method is a general concept where a solvent other than water is used, and the synthesis is usually performed at a temperature above the boiling temperature of the solvent in closed chemical reactors at higher pressures. Moreover, the greater pressure inside the closed reactor results in enhanced salt solubility. The benefits of the solvothermal process allowed researchers to develop reproducible protocols with total control of the long-term synthesis

processes. The solvothermal method has the advantage of higher product yield with improved crystallinity [130]. The hydrothermal/solvothermal method has been optimized for the synthesis of MOFs such as Ni-MOF [131], Co-MOF [131], Fe-MOF [132], Cu-MOF [133], Zn-MOF [134], and mixed-ligand metal-organic frameworks [135]. In recent years, electrochemical synthesis gained attention, and several MOFs such as $\text{Cu}_3(\text{HHTP})_2$ [136], Mn-DABDC(ES) [137], 2D/3D Zn(II)-MOF hybrid [138], Fe-MIL-101 and Fe-MIL-101-NH₂ [139], etc. have been reported for various MOFs' electrocatalytic applications. Electrochemical synthesis has the advantages of mild synthesis conditions, shorter synthesis times, and controllability of morphology and thickness by the applied current/voltage [140]. During electrochemical synthesis, the metal ions enter the solution through the dissolution of the anode and the process is usually continuous with the availability of dissolved linker molecules [141]. Researchers have also developed a variety of other synthesis approaches such as ultrasound and microwave-assisted [142], mechanochemical [143], and sonochemical [144] methods for the synthesis of MOFs with different morphology and applications (Figure 19). As shown in Table 4, modified MOF nanocomposites often outperform unmodified MOF and are often exploited for diverse biosensor applications [145]. MOFs are often decorated with metal nanoparticles in immunosensor applications for anchoring antibodies and enhancing the electrochemical signal. Nanoparticles decorated MOFs with versatile ligands and metal clusters, low cost, and simple operation provide researchers with an adequate 2D platform for biosensing applications. Li et al. [146] fabricated such an interesting immunosensor platform with core-shell $\text{Cu}_2\text{O}@ \text{Cu-MOF}@ \text{AuNPs}$ nanostructures for the sensitive detection of CEA (Figure 20A). Here, the sandwich-type electrochemical immunosensor achieved a tripled electrical signal amplification due to the synergistic effect of Cu-MOF, Cu_2O , and AuNPs. Nanowires had more surface area to accommodate proteins and were used to fabricate label-free sensors with exceptional performance [147,148]. Li et al. [149] constructed such an ultrasensitive label-free platform for the detection of NMP-22 based on CuAu nanowires decorated Co-MOFs (Figure 20B). The outstanding catalytic capabilities of Co-MOFs/CuAu NWs achieved a highly sensitive immunosensor with a good linear response (0.1 pg/mL–1 ng/mL), with a lower detection limit (33 fg/mL) suitable for the detection of NMP-22 from human urine samples. An immunoprobe based on AuNPs decorated Fe-MOF for the detection of PSA was reported by Feng et al. [150]. In this study, the labeling antibody was immobilized on AuNPs/Fe-MOF, and methylene blue (MB) covered by a thin layer of AuNPs-rGO served to covalently attach the coating antibodies. An amperometric signal at 0.18 V was measured to quantitatively measure PSA from urine samples (Figure 20C). Zhang et al. [27] reported a similar MB-based strategy for the detection of PSA (Figure 20D). Here, the MOF-325 adsorbed and stabilized MB, thereby solving the problem of MB leakage. A similar nanocomposite comprising MOF, rGO, and AuNPs was reported by Mehmandoust et al. [151] for the detection of a GFAP biomarker (Figure 20F). Here, AuNPs were anchored onto zeolitic imidazolate MOFs and were deployed as a recognition element for the detection of GFAP in urine samples. The intrinsic properties of unique nanomaterials are advantageous for specific immunosensor applications. Zhao et al. [152] fabricated an immunosensor for the detection of NMP-22 based on AuNPs and PtNPs decorated MOFs. The nanoparticles decorated MOF sowed an increased surface area to anchor antibodies through Pt-S and Au-N bonding (Figure 20E), and the immunosensor reported a sensitive response towards NMP-22.

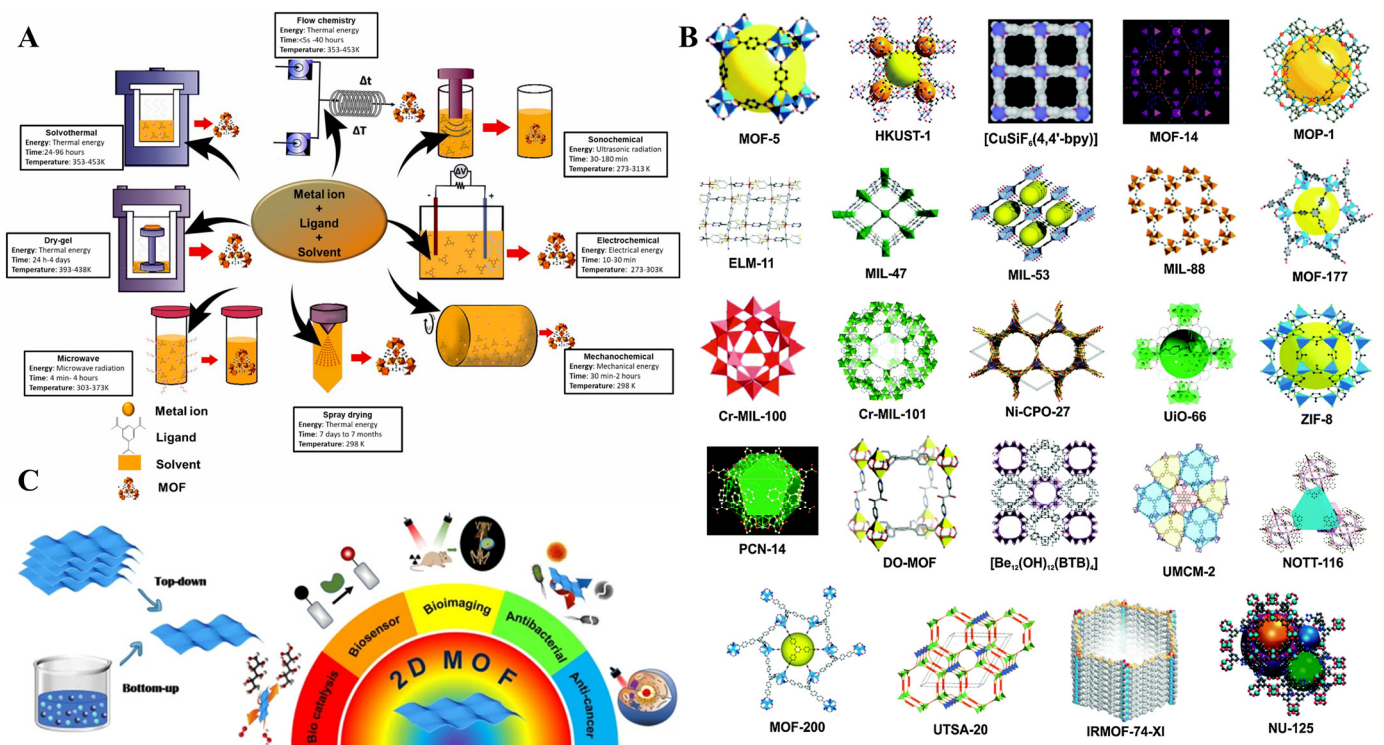


Figure 19. (A) Various literature reported conditions and approaches for the synthesis of MOFs. Reprinted with permission from Ref. [153]. Copyright 2021, Elsevier. (B) Structures of porous MOFs reported by several research groups. Reprinted with permission from Ref. [154]. Copyright 2015, Royal Society of Chemistry. (C) Various biomedical applications of 2D MOFs. Reprinted with permission from Ref. [155]. Copyright 2022, BMC (Springer).

Table 4. Recent literature reports on metal nanoparticles incorporated MOFs for electrochemical biomarker detection.

Sensing Platform	Biomarker	Technique	Linear Range	LOD	Real Sample	Ref.
Au/MOF-235/MB	PSA	DPV	0.01–1.2 ng/mL	3 pg/mL	Human serum	[28]
Co-MOFs/CuAu NWs	NMP-22	CA	10 ⁻⁴ –1 ng/mL	33 fg/mL	Human urine	[149]
AuNPs/Fe-MOF	PSA	SWV	0.001–100 ng/mL	0.13 pg/mL	Human serum	[150]
Au@ZIF-8@rGO/SPE	GFAP	EIS	50–10,000 fg/mL	50 fg/mL	Human urine	[151]
rGO-TEPA/AuNPs-PtNPs-MOFs	NMP-22	DPV	0.005–20 ng/mL	1.7 pg/mL	Human urine	[152]
PtNPs/Fe-MOF	Thrombin	DPV	1 fM–10 nM	0.33 fM	Human serum	[156]
Fe ₃ O ₄ @UiO-66/Cu@Au	cTnI	DPV	0.05–100 ng/mL	16 pg/mL	Human serum	[157]
SiO ₂ -Fc-COOH-Au/UiO-66-TB	PCT	DPV	1 pg/mL–100 ng/mL	0.3 pg/mL	Human serum	[158]
Au-MoS ₂ /MOF	NSE	CA	1 pg/mL–100 ng/mL	0.37 pg/mL	Human serum	[159]
AgNPs@Co/Ni-MOF	AFP	ECL	1 pg/mL–100 ng/mL	0.417 pg/mL	Human serum	[160]
BSA/Ab-AgNPs/CdS@MOF-5/PDDA/FTO	cTnI	ECL	0.01–1000 pg/mL	5.01 fg/mL	Human serum	[161]
Pd/NH ₂ -ZIF-67	PSA	CA	100 fg/mL–50 ng/mL	0.03 pg/mL	Human serum	[162]

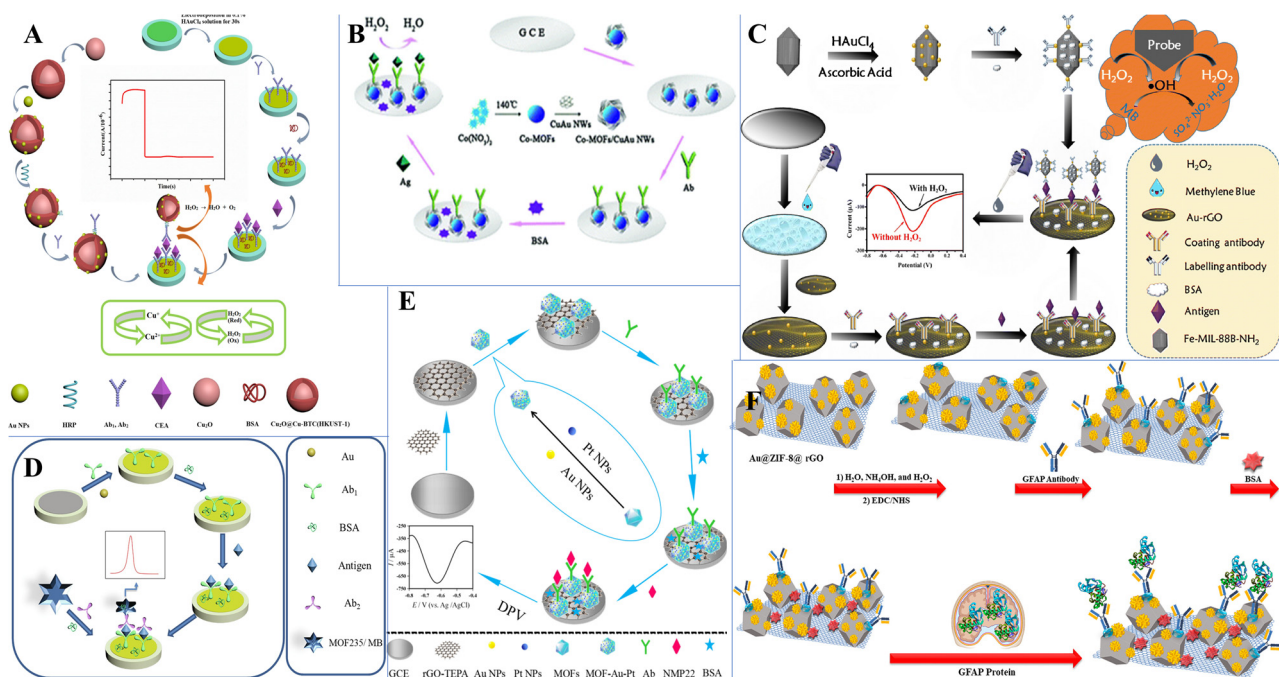


Figure 20. Schematic illustrations of (A) Fabrication of core-shell $\text{Cu}_2\text{O}@Cu\text{-MOF}@Au\text{NPs}$ -based electrochemical immunosensor for CEA detection. Reproduced with permission from Ref. [146]. Copyright 2020 Springer, (B) Preparation of Co-MOFs/CuAu NWs based label-free immunosensor for the detection of NMP-22. Reproduced with permission from Ref. [149]. Copyright 2019 Royal society of chemistry, (C) Fabrication of Au-MOF-based amperometric immunosensor for the detection of PSA. Reproduced with permission from Ref. [150]. Copyright 2020 Springer, (D) Preparation steps of AuNPs decorated MOF235/MB based electrochemical immunosensor for PSA detection. Reproduced with permission from Ref. [28]. Copyright 2021 Elsevier, (E) Stepwise assembly of AuNPs-PtNPs-MOFs based electrochemical immunosensor for the detection of NMP-22 in urine samples. Reproduced with permission from Ref. [152]. Copyright 2019 Elsevier, and (F) Preparation of GFAP-BSA-Anti-GFAP-Au@ZIF-8@rGO/SPE based electrochemical immunosensor for the detection of GFAP. Reproduced with permission from Ref. [151]. Copyright 2022 ACS.

2.5. Biomarker Detection on Other 2D Materials Conjugated with Metal Nanoparticles

2D materials such as graphitic carbon nitride, black phosphorous, 2D layered double hydroxides (LDHs), boron nitrides, graphdiyne, etc. have also been explored in conjunction with metal nanoparticles for immunosensor applications with interesting biomarker targets (Figure 21, Table 5). Graphdiyne, the new 2D carbon allotrope with its unique sp-sp² carbon network and highly π -conjugated structure has been receiving increased attention [163]. A graphdiyne-based self-powered biosensor platform was constructed by Hou et al. [164] for the determination of miRNA-21. Here, both the cathode and bioanode were fabricated by different modifications of AuNPs/GDY (Figure 21A). The 2D hexagonal boron nitride nanosheets, due to their electronic conductivity and large surface area were explored for immunosensor applications [165]. A label-free aptasensor for the detection of cardiac biomarker myoglobin on AuNPs decorated 2D-Boron nitride nanosheets was reported by Adeel et al. [166]. Here, the boron nitride nanosheets modified electrode AuNPs/BNNSs/FTO acted as a transducer for the immobilization of thiol-functionalized DNA aptamer for the specific binding of myoglobin (Figure 21B). Carbon nitrides are polymeric materials mainly consisting of carbon and nitrogen [167,168]. At ambient temperature, graphitic carbon nitride (g-C₃N₄) is the most stable allotrope of carbon nitrides. Due to the presence of basic surface groups and rich surface properties, g-C₃N₄ is attractive for many applications including catalysis [169]. Neto et al. [170] fabricated a miniaturized PEC system based on AuNPs decorated g-C₃N₄ for the detection of the breast cancer biomarker CA15-3 (Figure 21C). In this work, AuNPs on the g-C₃N₄ platform acted as a linker to

11-mercaptoundecanoic acid for the effective adsorption of antibodies. The performance of the PEC sensor was remarkable with a long linear range (0.1 fg/mL–10 ng/mL) and a very low detection limit (0.04 fg/mL). One of the promising candidates for immunosensor applications is 2D-Black phosphorus (BP) with high carrier mobility and controllable bandgap [171]. The unique properties of BP at atomic thickness are valuable for diverse applications [172–174]. Li et al. [175] reported a 2D-black phosphorous-supported Pt-Pd nanoelectrocatalyst for the determination of 4-AP, a potent biomarker for aniline exposure. Layered double hydroxides (LDHs) received attention because of their tunable chemistry and high charge density [176]. In one study, an electrochemical immunosensor based on AuNPs decorated ferrocene carboxylic acid conjugated MgAl layered double hydroxides for the label-free detection of CA-125 was reported by Wu et al. [177]. In this work, an LBL approach was used to increase the number of ferrocenes and antibodies, thereby amplifying the signal. The sensor reportedly displayed a wide linear range (0.01–1000 U/mL) and LOD (0.004 U/mL) and was tested for clinical cancer diagnostics (Figure 21D).

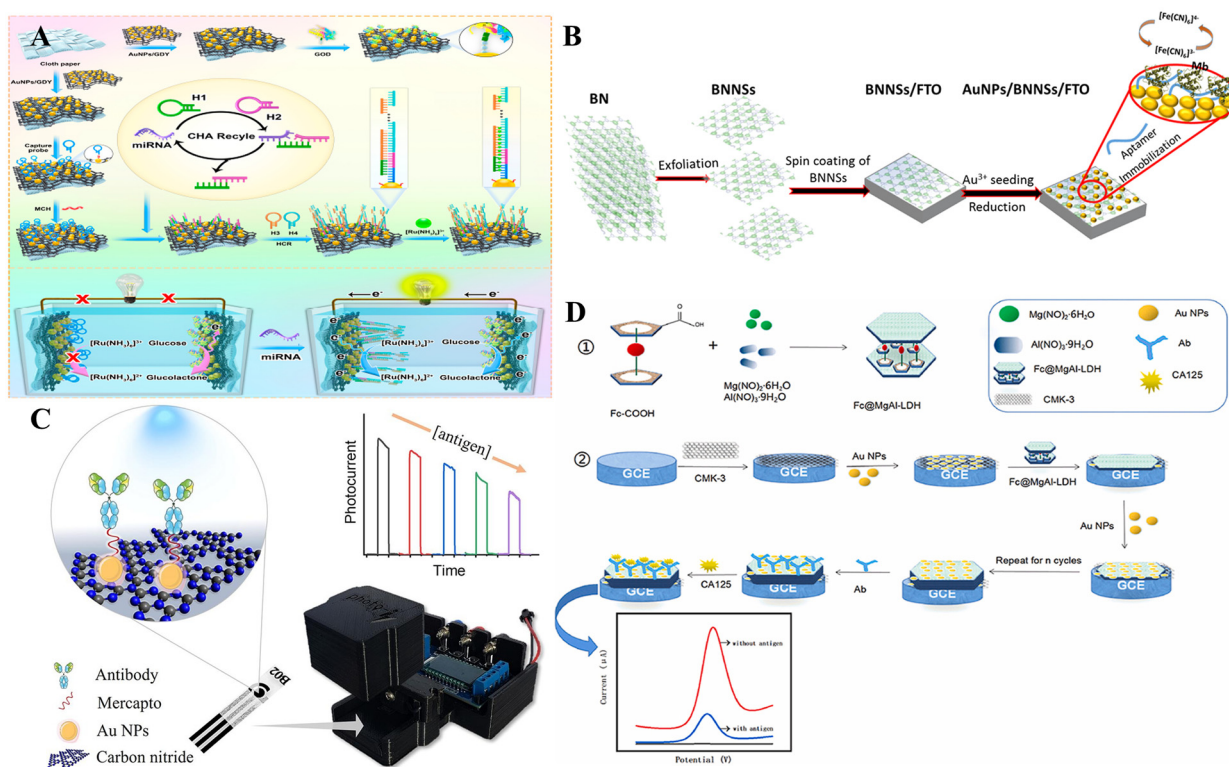


Figure 21. Schematic illustration of (A) Fabrication of a GDY-based self-powered device for miRNA-21 detection. Reprinted with permission from Ref. [164]. Copyright 2021 ACS, (B) Fabrication of AuNPs decorated boron nitride nanosheets based label-free aptasensor for the detection of the cardiac biomarker myoglobin. Reprinted with permission from Ref. [165]. Copyright 2019 Elsevier, (C) Graphitic carbon nitride sensitized with AuNPs for the PEC detection of CA15-3. Reprinted with permission from Ref. [170]. Copyright 2022 Elsevier, and (D) Fabrication of label-free electrochemical immunosensor based on LBL assembly of mesoporous carbon, AuNPs, and MgAl LDHs containing ferrocenecarboxylic acid. Reprinted with permission from Ref. [177]. Copyright 2022 Elsevier.

Table 5. Recent literature reports on biomarker detection based on various metal nanoparticles decorated 2D materials.

Sensing Platform	Biomarker	Technique	Linear Range	LOD	Real Sample	Ref.
AuNPs/GDY	miRNA-21	OCV	0.1–100,000 fM	0.034 fM	Human serum	[164]
Au-NPs/2D-hBN/FTO	Mb	DPV	0.1–100 µg/mL	34.6 ng/mL	Human serum	[166]
AuNPs-g-C ₃ N ₄	CA15-3	PEC	10 ⁻⁷ –10 ¹ ng/mL	0.04 fg/mL	Human serum	[170]
Pt-Pd/BP	4-AP	DPV	0.02–5 µM	14.1 nM	—	[175]
Au/Fc@MgAl-LDH	CA-125	DPV	0.01 U/mL–1000 U/mL	0.004 U/mL	Human serum	[177]
AuNRs-g-C ₃ N ₄	NS1	EIS	0.6–216 ng/mL	0.09 ng/mL	Human serum	[178]

3. Conclusions

In this review, we have discussed various electrochemical sensors that have been reported in recent years which incorporate various 2D nanomaterials conjugated with metal nanoparticles towards biomarker detection that have potential suitability for clinical use and some for point-of-care applications for cancer diagnosis. Although much research has been done in the synthesis of graphene, MoS₂, MXenes, MOFs, and other 2D materials incorporated with metal nanoparticles for an in vitro analysis of biomarkers. However, significant progress needs to be done in performing an in vivo analysis. Moreover, due to their inherent conductivity, these 2D nanomaterials are significantly used in electrochemical or even optical sensing. However, they are often doped with other nanomaterials to improve their electroactivity/conductivity. Further, new approaches such as nanofabrication and clinical applicability are most crucial for developing an open-use-dispose type of sensor at low cost. Furthermore, electrode-to-electrode variations upon modifications with nanomaterials largely depend on the type of functionalization method adopted, which also needed to be studied for developing electrochemical transducers with greater stability and reproducibility. Finally, the paper-based electrochemical and wearable electrochemical sensing approaches for biomarker detections are also promising due to their improved sensitivity, selectivity, and portability, such as a simple paper-based sensor that can measure with an application able to get the electrochemical signal downloaded into a smartphone is best suitable for clinical/point-of-care applications [179,180]. Though the integration of microfluidic devices with electrochemical systems possesses numerous advantages, including rapid manipulation of sample fluid, reduced reagent consumption, and low cost, commercialization of these electrochemical sensors is still in its infancy due to the challenges that these techniques are facing, such as miniaturization (multiple electrodes and channels) and integration of microfluidic systems (miniaturized flow controllers). Therefore, it is necessary to develop manufacturable biosensors that can provide accurate quantification of a biomarker of interest with a meager quantity of solutions at point-of-care with simple fabrication steps by avoiding multiple modifications on the electrode surface.

Author Contributions: A.K.: conceptualization, methodology, validation, writing—original draft preparation; A.K.Y.: conceptualization, methodology, validation, writing—original draft preparation; M.-H.L.: writing—review and editing, project administration, funding acquisition. All authors have read and agreed to the published version of the manuscript.

Funding: This work was supported by the Ministry of Trade, Industry, and Energy (Grant no. 20008763 and 20009860).

Institutional Review Board Statement: Not applicable.

Informed Consent Statement: Not applicable.

Data Availability Statement: Not applicable.

Conflicts of Interest: The authors declare no conflict of interest.

Abbreviations

2D	Two dimensional
2D-Hbn	2D-hexagonal boron nitride
AgNPs	Silver nanoparticles
AgNRs	Silver nanorods
Apt	Aptamer
Au	Gold
AuE	Gold electrode
AuNP-RGO	Au nanoparticle-reduced graphene oxide
AuNPs	Gold nanoparticles
AuPtBNPs	Gold platinum bimetallic nanoparticles
BDC	1,4-benzenedicarboxylate
BiVO ₄	Bismuth vanadate
BNNSs	Boron nitride nanosheets
BP	Black phosphorous
BSA	Bovine serum albumin
CA 27-29 BCA	Cancer antigen 27-29 breast cancer antigen
CA	Chronoamperometry
CA125	Cancer antigen 125
CA15-3	Cancer antigen 15-3
C-DNA	Capture DNA
CEA	Carcinoembryonic antigen
ce-MoS ₂	Chemical exfoliated MoS ₂
CGO	Carboxylic groups
CLB	Clenbuterol
CoPP	Cobalt protoporphyrin
CP	Capture probe
CPEB4	Cytoplasmic polyadenylate element-binding protein 4
Cr.6	18-crown-6
CRP	C-reactive protein
CS	Chitosan
CTnI	Cardiac troponin I
CTnT	Cardiac troponin T
CV	Cyclic voltammetry
CYFRA21-1	Cytokeratin 19 fragment
DNA	Deoxyribonucleic acid
DPV	Differential pulse voltammetry
ECD	Extracellular domain
ECL	Electrochemiluminescence
EIS	Electrochemical impedance spectroscopy
ELISA	Enzyme-linked immunosorbent assay
eT	Electron transfer
Fc	Ferrocene
FTO	Fluorine doped tin oxide
g-C ₃ N ₄	Graphitic carbon nitride
GCE	Glassy carbon electrode
GDY	Graphdiyne
GE	Graphite electrode
GFAP	Glial fibrillary acidic protein
GP120	Glycoprotein GP120
4-AP	p-Aminophenol
HER-2	Human epidermal growth factor receptor-2
HP1	Hairpin DNA
HT	Hexane thiol
IL8	Interleukin-8
i-t curve	Amperometric current-time response

ITO	Indium tin oxide
LA	Lactic acid
LBL	Layer by layer
L-cys	L-Cysteine
LOD	Limit of detection
LSV	Linear sweep voltammetry
L-Trp	L-tryptophan
Mb	Myoglobin
MCH	6-mercaptohexanol
MgAl-LDH	Mg-Al-Layered double hydroxide
MGMT	O6-methylguanine-DNA methyltransferase
miRNA-141	micro-RNA-141
miRNA-21	micro-RNA-21
miRNA-377	micro-RNA-377
miRNAs	micro-RNAs
MNPs	Mesoporous nanoparticles
MOFs	Metal organic frameworks
MUC1	Mucin1
MWCNT	Multiwalled carbon nanotubes
NMP-22	Nuclear matrix protein 22
NS1	Non-structural 1
NSE	Neuron-specific enolase
OCV	Open circuit voltage
OTC	Oxytetracycline
PAMAM	Polyamidoamine
PCT	Procalcitonin
PDA	Polydopamine
PdPtBP MNPs	Pd-Pt-Black phosphorous-mesoporous nanoparticles
PEC	Photoelectrochemical
PET	Polyethylene terephthalate
PPY	Polypyrrole
PSA	Prostate specific antigen
PtNPs	Platinum nanoparticles
RAC	Ractopamine
rGO	Reduced graphene oxide
RhNPs	Rhodium nanoparticles
RNA	Ribonucleic acid
S/N	Signal-to-noise ratio
SAL	Salbutamol
SPCE	Screen-printed carbon electrode
SWV	Square wave voltammetry
TEPA	Tetraethylenepentamine
VEGF165	Vascular endothelial growth factor 165
YNCs	Yolk-shell nanocubes
β -CD	β -cyclodextrin

References

1. Filice, M.; Ruiz-Cabello, J. *Nucleic Acid Nanotheranostics: Biomedical Applications*; Elsevier: Amsterdam, The Netherlands, 2019.
2. WHO. *Biomarkers in Risk Assessment: Validity and Validation-Environmental Health Criteria 222*; WHO: Geneva, Switzerland, 2001.
3. National Cancer Institute. Biomarker. Available online: <https://www.cancer.gov/publications/dictionaries/cancer-terms/def/biomarker> (accessed on 5 October 2022).
4. Biomarkers Definitions Working Group. Biomarkers and surrogate endpoints: Preferred definitions and conceptual framework. *Clin. Pharmacol. Ther.* **2001**, *69*, 89–95. [[CrossRef](#)]
5. Kikkeri, K.; Wu, D.; Voldman, J. A sample-to-answer electrochemical biosensor system for biomarker detection. *Lab Chip* **2022**, *22*, 100–107. [[CrossRef](#)] [[PubMed](#)]
6. Ziemssen, T.; Akgün, K.; Brück, W. Molecular biomarkers in multiple sclerosis. *J. Neuroinflamm.* **2019**, *16*, 272. [[CrossRef](#)] [[PubMed](#)]

7. Pachner, A.R.; DiSano, K.; Royce, D.B.; Gilli, F. Clinical utility of a molecular signature in inflammatory demyelinating disease. *Neurol. Neuroimmunol. Neuroinflamm.* **2019**, *6*, e520. [CrossRef] [PubMed]
8. Sant, G.R.; Knopf, K.B.; Albala, D.M. Live-single-cell phenotypic cancer biomarkers-future role in precision oncology? *NPJ Precis. Oncol.* **2017**, *1*, 21. [CrossRef] [PubMed]
9. Huss, R. Chapter 19—Biomarkers. In *Translational Regenerative Medicine*; Atala, A., Allickson, J.G., Eds.; Academic Press: Boston, MA, USA, 2015; pp. 235–241.
10. Manzanares, J.; Sala, F.; Gutiérrez, M.S.G.; Rueda, F.N. 2.30—Biomarkers. In *Comprehensive Pharmacology*; Kenakin, T., Ed.; Elsevier: Oxford, UK, 2022; pp. 693–724.
11. Goossens, N.; Nakagawa, S.; Sun, X.; Hoshida, Y. Cancer biomarker discovery and validation. *Transl. Cancer Res.* **2015**, *4*, 256.
12. Califf, R.M. Biomarker definitions and their applications. *Exp. Biol. Med.* **2018**, *243*, 213–221. [CrossRef]
13. FDA-NIH Biomarker Working Group. BEST (Biomarkers, Endpoints, and Other Tools). Available online: <https://www.ncbi.nlm.nih.gov/books/NBK326791/> (accessed on 7 November 2022).
14. Magar, H.S.; Hassan, R.Y.A.; Mulchandani, A. Electrochemical Impedance Spectroscopy (EIS): Principles, Construction, and Biosensing Applications. *Sensors* **2021**, *21*, 6578. [CrossRef]
15. Bertok, T.; Lorencova, L.; Chocholova, E.; Jane, E.; Vikartovska, A.; Kasak, P.; Tkac, J. Electrochemical Impedance Spectroscopy Based Biosensors: Mechanistic Principles, Analytical Examples and Challenges towards Commercialization for Assays of Protein Cancer Biomarkers. *ChemElectroChem* **2019**, *6*, 989–1003. [CrossRef]
16. Lisdat, F.; Schafer, D. The use of electrochemical impedance spectroscopy for biosensing. *Anal. Bioanal. Chem.* **2008**, *391*, 1555–1567. [CrossRef]
17. Grieshaber, D.; MacKenzie, R.; Voros, J.; Reimhult, E. Electrochemical biosensors—Sensor principles and architectures. *Sensors* **2008**, *8*, 1400–1458. [CrossRef]
18. Rezaei, B.; Irannejad, N. Chapter 2—Electrochemical detection techniques in biosensor applications. In *Electrochemical Biosensors*; Ensafi, A.A., Ed.; Elsevier: Amsterdam, The Netherlands, 2019; pp. 11–43.
19. Speiser, B. Electroanalytical Methods. 2. Cyclic Voltammetry. *Chem. Unserer. Zeit.* **1981**, *15*, 62–67. [CrossRef]
20. Huan, T.N.; Ha, V.T.T.; Hung, L.Q.; Yoon, M.Y.; Han, S.H.; Chung, H. Square wave voltammetric detection of Anthrax utilizing a peptide for selective recognition of a protein biomarker. *Biosens. Bioelectron.* **2009**, *25*, 469–474. [CrossRef]
21. Kumar, S.; Kalkal, A. 3—Electrochemical detection: Cyclic voltammetry/differential pulse voltammetry/impedance spectroscopy. In *Nanotechnology in Cancer Management*; Khondakar, K.R., Kaushik, A.K., Eds.; Elsevier: Amsterdam, The Netherlands, 2021; pp. 43–71.
22. Moore, S. Current Global Market of 2D Materials. Available online: <https://www.azonano.com/article.aspx?ArticleID=6294> (accessed on 26 December 2022).
23. Popov, A.; Brasiunas, B.; Kausaite-Minkstimiene, A.; Ramanaviciene, A. Metal Nanoparticle and Quantum Dot Tags for Signal Amplification in Electrochemical Immunosensors for Biomarker Detection. *Chemosensors* **2021**, *9*, 85. [CrossRef]
24. Enoch, I.V.M.V.; Ramasamy, S.; Mohiyuddin, S.; Gopinath, P.; Manoharan, R. Cyclodextrin-PEG conjugate-wrapped magnetic ferrite nanoparticles for enhanced drug loading and release. *Appl. Nanosci.* **2018**, *8*, 273–284. [CrossRef]
25. Liu, Y.; Yang, G.; Jin, S.; Xu, L.; Zhao, C.X. Development of high-drug-loading nanoparticles. *ChemPlusChem* **2020**, *85*, 2143–2157. [CrossRef]
26. Aido, A.; Wajant, H.; Buzgo, M.; Simaite, A. Development of anti-TNFR antibody-conjugated nanoparticles. *Multidiscip. Digit. Publ. Inst. Proc.* **2020**, *78*, 55.
27. Li, Y.; Wang, Y.; Zhang, N.; Fan, D.; Liu, L.; Yan, T.; Yang, X.; Ding, C.; Wei, Q.; Ju, H. Magnetic electrode-based electrochemical immunosensor using amorphous bimetallic sulfides of CoSnS_x as signal amplifier for the NTpro BNP detection. *Biosens. Bioelectron.* **2019**, *131*, 250–256. [CrossRef]
28. Zhang, M.; Hu, X.; Mei, L.; Zhang, L.; Wang, X.; Liao, X.; Qiao, X.; Hong, C. PSA detection electrochemical immunosensor based on MOF-235 nanomaterial adsorption aggregation signal amplification strategy. *Microchem. J.* **2021**, *171*, 106870. [CrossRef]
29. Wang, H.; Zhang, S.; Li, S.; Qu, J. Electrochemical sensor based on palladium-reduced graphene oxide modified with gold nanoparticles for simultaneous determination of acetaminophen and 4-aminophenol. *Talanta* **2018**, *178*, 188–194. [CrossRef]
30. Lim, J.Y.; Mubarak, N.M.; Abdullah, E.C.; Nizamuddin, S.; Khalid, M.; Inamuddin. Recent trends in the synthesis of graphene and graphene oxide based nanomaterials for removal of heavy metals—A review. *J. Ind. Eng. Chem.* **2018**, *66*, 29–44. [CrossRef]
31. Mbayachi, V.B.; Ndayiragije, E.; Sammani, T.; Taj, S.; Mbuta, E.R.; Khan, A.U. Graphene synthesis, characterization and its applications: A review. *Results Chem.* **2021**, *3*, 100163. [CrossRef]
32. Bhuyan, M.S.A.; Uddin, M.N.; Islam, M.M.; Bipasha, F.A.; Hossain, S.S. Synthesis of graphene. *Int. Nano Lett.* **2016**, *6*, 65–83. [CrossRef]
33. Singh, R.K.; Kumar, R.; Singh, D.P. Graphene oxide: Strategies for synthesis, reduction and frontier applications. *RSC Adv.* **2016**, *6*, 64993–65011. [CrossRef]
34. Yagati, A.K.; Behrent, A.; Beck, S.; Rink, S.; Goepferich, A.M.; Min, J.; Lee, M.H.; Baeumner, A.J. Laser-induced graphene interdigitated electrodes for label-free or nanolabel-enhanced highly sensitive capacitive aptamer-based biosensors. *Biosens. Bioelectron.* **2020**, *164*, 112272. [CrossRef]
35. Ranjan, P.; Sadique, M.A.; Yadav, S.; Khan, R. An Electrochemical Immunosensor Based on Gold-Graphene Oxide Nanocomposites with Ionic Liquid for Detecting the Breast Cancer CD44 Biomarker. *ACS Appl. Mater. Inter.* **2022**, *14*, 20802–20812. [CrossRef]

36. Yagati, A.K.; Pyun, J.C.; Min, J.; Cho, S. Label-free and direct detection of C-reactive protein using reduced graphene oxide-nanoparticle hybrid impedimetric sensor. *Bioelectrochemistry* **2016**, *107*, 37–44. [[CrossRef](#)]
37. Jonous, Z.A.; Shayeh, J.S.; Yazdian, F.; Yadegari, A.; Hashemi, M.; Omidi, M. An electrochemical biosensor for prostate cancer biomarker detection using graphene oxide-gold nanostructures. *Eng. Life Sci.* **2019**, *19*, 206–216. [[CrossRef](#)]
38. Kasturi, S.; Eom, Y.; Torati, R.; Kim, C. Highly sensitive electrochemical biosensor based on naturally reduced rGO/Au nanocomposite for the detection of miRNA-122 biomarker. *J. Ind. Eng. Chem.* **2021**, *93*, 186–195. [[CrossRef](#)]
39. Rauf, S.; Lahcen, A.A.; Aljedaibi, A.; Beduk, T.; de Oliveira, J.I.; Salama, K.N. Gold nanostructured laser-scribed graphene: A new electrochemical biosensing platform for potential point-of-care testing of disease biomarkers. *Biosens. Bioelectron.* **2021**, *180*, 113116. [[CrossRef](#)]
40. Hasanjani, H.R.A.; Zarei, K. DNA/Au-Pt bimetallic nanoparticles/graphene oxide-chitosan composites modified pencil graphite electrode used as an electrochemical biosensor for sub-picomolar detection of anti-HIV drug zidovudine. *Microchem. J.* **2021**, *164*, 106005. [[CrossRef](#)]
41. Kanagavalli, P.; Veerapandian, M. Opto-electrochemical functionality of Ru(II)-reinforced graphene oxide nanosheets for immunosensing of dengue virus non-structural 1 protein. *Biosens. Bioelectron.* **2020**, *150*, 111878. [[CrossRef](#)] [[PubMed](#)]
42. Kanagavalli, P.; Andrew, C.; Veerapandian, M.; Jayakumar, M. In-situ redox-active hybrid graphene platform for label-free electrochemical biosensor: Insights from electrodeposition and electroless deposition. *TrAC-Trend Anal. Chem.* **2021**, *143*, 116413. [[CrossRef](#)]
43. Liang, Y.; Xu, Y.; Tong, Y.Y.; Chen, Y.; Chen, X.L.; Wu, S.M. Graphene-Based Electrochemical Sensor for Detection of Hepatocellular Carcinoma Markers. *Front. Chem.* **2022**, *10*, 883627. [[CrossRef](#)] [[PubMed](#)]
44. Ozkan-Ariksoysal, D. Current Perspectives in Graphene Oxide-Based Electrochemical Biosensors for Cancer Diagnostics. *Biosensors* **2022**, *12*, 607. [[CrossRef](#)]
45. Rashid, J.I.A.; Kannan, V.; Ahmad, M.H.; Mon, A.A.; Taufik, S.; Miskon, A.; Ong, K.K.; Yusof, N.A. An electrochemical sensor based on gold nanoparticles-functionalized reduced graphene oxide screen printed electrode for the detection of pyocyanin biomarker in *Pseudomonas aeruginosa* infection. *Mat. Sci. Eng. C Mater.* **2021**, *120*, 111625. [[CrossRef](#)]
46. Abolhasan, R.; Khalilzadeh, B.; Yousefi, H.; Samemaleki, S.; Chakari-Khiavi, F.; Ghorbani, F.; Pourakbari, R.; Kamrani, A.; Khataee, A.; Rad, T.S.; et al. Ultrasensitive and label free electrochemical immunosensor for detection of ROR1 as an oncofetal biomarker using gold nanoparticles assisted LDH/rGO nanocomposite. *Sci. Rep.* **2021**, *11*, 14921. [[CrossRef](#)]
47. Liu, X.K.; Lin, L.Y.; Tseng, F.Y.; Tan, Y.C.; Li, J.; Feng, L.; Song, L.J.; Lai, C.F.; Li, X.H.; He, J.H.; et al. Label-free electrochemical immunosensor based on gold nanoparticle/polyethyleneimine/reduced graphene oxide nanocomposites for the ultrasensitive detection of cancer biomarker matrix metalloproteinase-1. *Analyst* **2021**, *146*, 4066–4079. [[CrossRef](#)]
48. Ye, S.; Liu, Y.; Zeng, M.; Feng, W.; Yang, H.; Zheng, X. Electrochemical Immunoassay of Melanoma Biomarker CPEB4 Based on Cobalt Porphyrin Functionalized Graphene Oxide. *J. Electrochem. Soc.* **2022**, *169*, 027510. [[CrossRef](#)]
49. Yagati, A.K.; Lee, G.Y.; Ha, S.; Chang, K.A.; Pyun, J.C.; Cho, S. Impedimetric Tumor Necrosis Factor-alpha Sensor Based on a Reduced Graphene Oxide Nanoparticle-Modified Electrode Array. *J. Nanosci. Nanotechnol.* **2016**, *16*, 11921–11927. [[CrossRef](#)]
50. Ben Moussa, F.; Achi, F.; Meskher, H.; Henni, A.; Belkhalifa, H. Green one-step reduction approach to prepare rGO@AgNPs coupled with molecularly imprinted polymer for selective electrochemical detection of lactic acid as a cancer biomarker. *Mater. Chem. Phys.* **2022**, *289*, 126456. [[CrossRef](#)]
51. Wang, H.; Zhang, Y.; Li, H.; Du, B.; Ma, H.M.; Wu, D.; Wei, Q. A silver-palladium alloy nanoparticle-based electrochemical biosensor for simultaneous detection of ractopamine, clenbuterol and salbutamol. *Biosens. Bioelectron.* **2013**, *49*, 14–19. [[CrossRef](#)] [[PubMed](#)]
52. Akbarzadeh, S.; Khajehsharifi, H.; Hajihosseini, S. Detection of Oxytetracycline Using an Electrochemical Label-Free Aptamer-Based Biosensor. *Biosensors* **2022**, *12*, 468. [[CrossRef](#)] [[PubMed](#)]
53. Yang, H.; Ren, J.; Zhao, M.; Chen, C.; Wang, F.; Chen, Z. Novel electrochemical immunosensor for O⁶-methylguanine-DNA methyltransferase gene methylation based on graphene oxide-magnetic nanoparticles-β-cyclodextrin nanocomposite. *Bioelectrochemistry* **2022**, *146*, 108111. [[CrossRef](#)]
54. Pothipor, C.; Jakmune, J.; Bamrungsap, S.; Ounnunkad, K. An electrochemical biosensor for simultaneous detection of breast cancer clinically related microRNAs based on a gold nanoparticles/graphene quantum dots/graphene oxide film. *Analyst* **2021**, *146*, 4000–4009. [[CrossRef](#)]
55. Sadeghi, M.; Kashanian, S.; Naghib, S.M.; Arkan, E. A high-performance electrochemical aptasensor based on graphene-decorated rhodium nanoparticles to detect HER2-ECD oncomarker in liquid biopsy. *Sci. Rep.* **2022**, *12*, 3299. [[CrossRef](#)]
56. Verma, S.; Singh, A.; Shukla, A.; Kaswan, J.; Arora, K.; Ramirez-Vick, J.; Singh, P.; Singh, S.P. Anti-IL8/AuNPs-rGO/ITO as an Immunosensing Platform for Noninvasive Electrochemical Detection of Oral Cancer. *ACS Appl. Mater. Inter.* **2017**, *9*, 27462–27474. [[CrossRef](#)]
57. Barman, S.C.; Hossain, M.F.; Yoon, H.; Park, J.Y. Trimetallic Pd@Au@Pt nanocomposites platform on -COOH terminated reduced graphene oxide for highly sensitive CEA and PSA biomarkers detection. *Biosens. Bioelectron.* **2018**, *100*, 16–22. [[CrossRef](#)]
58. Thunkhamrak, C.; Chuntib, P.; Ounnunkad, K.; Banet, P.; Aubert, P.H.; Saianand, G.; Gopalan, A.I.; Jakmune, J. Highly sensitive voltammetric immunosensor for the detection of prostate specific antigen based on silver nanoprobe assisted graphene oxide modified screen printed carbon electrode. *Talanta* **2020**, *208*, 120389. [[CrossRef](#)]

59. Khoshnevisan, K.; Torabi, F.; Baharifar, H.; Sajjadi-Jazi, S.M.; Afjeh, M.S.; Faridbod, F.; Larijani, B.; Khorramizadeh, M.R. Determination of the biomarker L-tryptophan level in diabetic and normal human serum based on an electrochemical sensing method using reduced graphene oxide/gold nanoparticles/18-crown-6. *Anal. Bioanal. Chem.* **2020**, *412*, 3615–3627. [[CrossRef](#)]
60. Meng, F.Y.; Sun, H.X.; Huang, Y.; Tang, Y.G.; Chen, Q.; Miao, P. Peptide cleavage-based electrochemical biosensor coupling graphene oxide and silver nanoparticles. *Anal. Chim. Acta* **2019**, *1047*, 45–51. [[CrossRef](#)] [[PubMed](#)]
61. Sangili, A.; Kalyani, T.; Chen, S.M.; Nanda, A.; Jana, S.K. Label-Free Electrochemical Immunosensor Based on One-Step Electrochemical Deposition of AuNP-RGO Nanocomposites for Detection of Endometriosis Marker CA 125. *ACS Appl. Bio Mater.* **2020**, *3*, 7620–7630. [[CrossRef](#)] [[PubMed](#)]
62. Rostamabadi, P.F.; Heydari-Bafrooei, E. Impedimetric aptasensing of the breast cancer biomarker HER2 using a glassy carbon electrode modified with gold nanoparticles in a composite consisting of electrochemically reduced graphene oxide and single-walled carbon nanotubes. *Microchim. Acta* **2019**, *186*, 495. [[CrossRef](#)] [[PubMed](#)]
63. Bharti, A.; Rana, S.; Dahiya, D.; Agnihotri, N.; Prabhakar, N. An electrochemical aptasensor for analysis of MUC1 using gold platinum bimetallic nanoparticles deposited carboxylated graphene oxide. *Anal. Chim. Acta* **2020**, *1097*, 186–195. [[CrossRef](#)] [[PubMed](#)]
64. Kumar, A.; Purohit, B.; Mahato, K.; Mandal, R.; Srivastava, A.; Chandra, P. Gold-Iron Bimetallic Nanoparticles Impregnated Reduced Graphene Oxide Based Nanosensor for Label-Free Detection of Biomarker Related to Non-Alcoholic Fatty Liver Disease. *Electroanalysis* **2019**, *31*, 2417–2428. [[CrossRef](#)]
65. Hu, H.W.; Zavabeti, A.; Quan, H.Y.; Zhu, W.Q.; Wei, H.Y.; Chen, D.C.; Ou, J.Z. Recent advances in two-dimensional transition metal dichalcogenides for biological sensing. *Biosens. Bioelectron.* **2019**, *142*, 111573. [[CrossRef](#)]
66. Subbaiah, Y.P.V.; Saji, K.J.; Tiwari, A. Atomically Thin MoS₂: A Versatile Nongraphene 2D Material. *Adv. Funct. Mater.* **2016**, *26*, 2046–2069. [[CrossRef](#)]
67. Kalantar-zadeh, K.; Ou, J.Z. Biosensors Based on Two-Dimensional MoS₂. *ACS Sens.* **2016**, *1*, 5–16. [[CrossRef](#)]
68. Van, T.D.; Thuy, N.D.T.; Phuong, T.D.V.; Thi, N.N.; Thi, T.N.; Phuong, T.N.; Van, T.V.; Vuong-Pham, H.; Dinh, T.P. High-performance nonenzymatic electrochemical glucose biosensor based on AgNP-decorated MoS₂ microflowers. *Curr. Appl. Phys.* **2022**, *43*, 116–123. [[CrossRef](#)]
69. Cui, Z.L.; Li, D.J.; Yang, W.H.; Fan, K.; Liu, H.Y.; Wen, F.; Li, L.L.; Dong, L.X.; Wang, G.F.; Wu, W. An electrochemical biosensor based on few-layer MoS₂ nanosheets for highly sensitive detection of tumor marker ctDNA. *Anal. Methods* **2022**, *14*, 1956–1962. [[CrossRef](#)]
70. Li, L.; Zhang, D.; Gao, Y.H.; Deng, J.P.; Gou, Y.C.; Fang, J.F. Electric field driven exfoliation of MoS₂. *J. Alloys Compd.* **2021**, *862*, 158551. [[CrossRef](#)]
71. Shi, Z.T.; Zhao, H.B.; Chen, X.Q.; Wu, G.M.; Wei, F.; Tu, H.L. Chemical vapor deposition growth and transport properties of MoS₂-2H thin layers using molybdenum and sulfur as precursors. *Rare Met.* **2022**, *41*, 3574–3578. [[CrossRef](#)]
72. Jagannadham, K.; Das, K.; Reynolds, C.L.; El-Masry, N. Nature of electrical conduction in MoS₂ films deposited by laser physical vapor deposition. *J. Mater. Sci. Mater. Electron.* **2018**, *29*, 14180–14191. [[CrossRef](#)]
73. Gomes, F.O.V.; Pokle, A.; Marinkovic, M.; Balster, T.; Canavan, M.; Fleischer, K.; Anselmann, R.; Nicolosi, V.; Wagner, V. Influence of temperature on morphological and optical properties of MoS₂ layers as grown based on solution processed precursor. *Thin Solid Films* **2018**, *645*, 38–44. [[CrossRef](#)]
74. Shah, S.A.; Khan, I.; Yuan, A.H. MoS₂ as a Co-Catalyst for Photocatalytic Hydrogen Production: A Mini Review. *Molecules* **2022**, *27*, 3289. [[CrossRef](#)] [[PubMed](#)]
75. Li, X.; Zhu, H. Two-dimensional MoS₂: Properties, preparation, and applications. *J. Mater.* **2015**, *1*, 33–44. [[CrossRef](#)]
76. Sinha, A.; Dhanjai, Tan, B.; Huang, Y.J.; Zhao, H.M.; Dang, X.M.; Chen, J.P.; Jain, R. MoS₂ nanostructures for electrochemical sensing of multidisciplinary targets: A review. *TrAC-Trend Anal. Chem.* **2018**, *102*, 75–90. [[CrossRef](#)]
77. Yagati, A.K.; Go, A.; Vu, N.H.; Lee, M.H. A MoS₂-Au nanoparticle-modified immunosensor for T-3 biomarker detection in clinical serum samples. *Electrochim. Acta* **2020**, *342*, 136065. [[CrossRef](#)]
78. Su, S.; Sun, H.F.; Cao, W.F.; Chao, J.; Peng, H.Z.; Zuo, X.L.; Yuwen, L.H.; Fan, C.H.; Wang, L.H. Dual-Target Electrochemical Biosensing Based on DNA Structural Switching on Gold Nanoparticle-Decorated MoS₂ Nanosheets. *ACS Appl. Mater. Int.* **2016**, *8*, 6826–6833. [[CrossRef](#)]
79. Chen, M.; Zhao, L.; Wu, D.; Tu, S.; Chen, C.; Guo, H.; Xu, Y. Highly sensitive sandwich-type immunosensor with enhanced electrocatalytic durian-shaped MoS₂/AuPtPd nanoparticles for human growth differentiation factor-15 detection. *Anal. Chim. Acta* **2022**, *1223*, 340194. [[CrossRef](#)]
80. Nong, C.J.; Yang, B.; Li, X.K.; Feng, S.X.; Cui, H.X. An ultrasensitive electrochemical immunosensor based on in-situ growth of CuWO₄ nanoparticles on MoS₂ and chitosan-gold nanoparticles for cortisol detection. *Microchem. J.* **2022**, *179*, 107434. [[CrossRef](#)]
81. Su, S.; Sun, Q.; Wan, L.; Gu, X.; Zhu, D.; Zhou, Y.; Chao, J.; Wang, L. Ultrasensitive analysis of carcinoembryonic antigen based on MoS₂-based electrochemical immunosensor with triple signal amplification. *Biosens. Bioelectron.* **2019**, *140*, 111353. [[CrossRef](#)]
82. Ma, N.; Zhang, T.; Fan, D.W.; Kuang, X.; Ali, A.; Wu, D.; Wei, Q. Triple amplified ultrasensitive electrochemical immunosensor for alpha fetoprotein detection based on MoS₂@Cu₂O-Au nanoparticles. *Sens. Actuators B Chem.* **2019**, *297*, 126821. [[CrossRef](#)]
83. Dalila, R.N.; Arshad, M.K.M.; Gopinath, S.C.B.; Ibaou, C.; Nuzaihan, M.M.N.; Fathil, M.F.M.; Azmi, U.Z.M.; Anbu, P. Faradaic electrochemical impedimetric analysis on MoS₂/Au-NPs decorated surface for C-reactive protein detection. *J. Taiwan Inst. Chem. E* **2022**, *138*, 104450. [[CrossRef](#)]

84. Xu, W.; Fei, J.W.; Yang, W.; Zheng, Y.N.; Dai, Y.; Sakran, M.; Zhang, J.; Zhu, W.Y.; Hong, J.L.; Zhou, X.M. A colorimetric/electrochemical dual-mode sensor based on Fe₃O₄@MoS₂-Au NPs for high-sensitivity detection of hydrogen peroxide. *Microchem. J.* **2022**, *181*, 107825. [[CrossRef](#)]
85. Shin, M.; Yoon, J.; Yi, C.Y.; Lee, T.; Choi, J.W. Flexible HIV-1 Biosensor Based on the Au/MoS₂ Nanoparticles/Au Nanolayer on the PET Substrate. *Nanomaterials* **2019**, *9*, 76. [[CrossRef](#)]
86. Li, S.; Zhang, J.W.; Tan, C.S.; Chen, C.; Hu, C.; Bai, Y.C.; Ming, D. Electrochemical immunosensor based on hybrid MoS₂/Pt@Au-nanoprism/PDA for simultaneous detection of free and total prostate specific antigen in serum. *Sens. Actuators B Chem.* **2022**, *357*, 131413. [[CrossRef](#)]
87. Ma, E.H.; Wang, P.; Yang, Q.S.; Yu, H.X.; Pei, F.B.; Li, Y.Y.; Liu, Q.; Dong, Y.H. Electrochemical immunosensor based on MoS₂ NFs/Au@AgPt YNCs as signal amplification label for sensitive detection of CEA. *Biosens. Bioelectron.* **2019**, *142*, 111580. [[CrossRef](#)]
88. Zhao, H.; Du, X.; Dong, H.; Jin, D.L.; Tang, F.; Liu, Q.; Wang, P.; Chen, L.; Zhao, P.Q.; Li, Y.Y. Electrochemical immunosensor based on Au/Co-BDC/MoS₂ and DPCN/MoS₂ for the detection of cardiac troponin I. *Biosens. Bioelectron.* **2021**, *175*, 112883. [[CrossRef](#)]
89. Alarfaj, N.A.; El-Tohamy, M.F.; Oraby, H. New label-free ultrasensitive electrochemical immunosensor-based Au/MoS₂/rGO nanocomposites for CA 27-29 breast cancer antigen detection. *New J. Chem.* **2018**, *42*, 11046–11053. [[CrossRef](#)]
90. Wang, X.; Chu, C.C.; Shen, L.; Deng, W.P.; Yan, M.; Ge, S.G.; Yu, J.H.; Song, X.R. An ultrasensitive electrochemical immunosensor based on the catalytic activity of MoS₂-Au composite using Ag nanospheres as labels. *Sens. Actuators B Chem.* **2015**, *206*, 30–36. [[CrossRef](#)]
91. Gui, J.C.; Han, L.; Du, C.X.; Yu, X.N.; Hu, K.; Li, L.H. An efficient label-free immunosensor based on ce-MoS₂/AgNR composites and screen-printed electrodes for PSA detection. *J. Solid State Electrochem.* **2021**, *25*, 973–982. [[CrossRef](#)]
92. Fan, Z.Q.; Yao, B.; Ding, Y.D.; Xie, M.H.; Zhao, J.F.; Zhang, K.; Huang, W. Electrochemiluminescence aptasensor for Siglec-5 detection based on MoS₂@Au nanocomposites emitter and exonuclease III-powered DNA walker. *Sens. Actuators B Chem.* **2021**, *334*, 129592. [[CrossRef](#)] [[PubMed](#)]
93. Ma, K.X.; Sinha, A.; Dang, X.M.; Zhao, H.M. Electrochemical Preparation of Gold Nanoparticles-Polypyrrole Co-Decorated 2D MoS₂ Nanocomposite Sensor for Sensitive Detection of Glucose. *J. Electrochem. Soc.* **2019**, *166*, B147–B154. [[CrossRef](#)]
94. Zhu, X.N.; Wang, Z.G.; Gao, M.Y.; Wang, Y.Q.; Hu, J.; Song, Z.X.; Wang, Z.B.; Dong, M.D. AgPt/MoS₂ hybrid as electrochemical sensor for detecting H₂O₂ release from living cells. *New J. Chem.* **2022**, *46*, 15032–15041. [[CrossRef](#)]
95. Kim, H.; Wang, Z.; Alshareef, H.N. MXetronics: Electronic and photonic applications of MXenes. *Nano Energy* **2019**, *60*, 179–197. [[CrossRef](#)]
96. Palisaitis, J.; Persson, I.; Halim, J.; Rosen, J.; Persson, P.O. On the structural stability of MXene and the role of transition metal adatoms. *Nanoscale* **2018**, *10*, 10850–10855. [[CrossRef](#)]
97. Mehdi Aghaei, S.; Aasi, A.; Panchapakesan, B. Experimental and theoretical advances in MXene-based gas sensors. *ACS Omega* **2021**, *6*, 2450–2461. [[CrossRef](#)]
98. Ibrahim, Y.; Mohamed, A.; Abdelgawad, A.M.; Eid, K.; Abdullah, A.M.; Elzatahry, A. The recent advances in the mechanical properties of self-standing two-dimensional MXene-based nanostructures: Deep insights into the supercapacitor. *Nanomaterials* **2020**, *10*, 1916. [[CrossRef](#)]
99. Fu, B.; Sun, J.; Wang, C.; Shang, C.; Xu, L.; Li, J.; Zhang, H. MXenes: Synthesis, optical properties, and applications in ultrafast photonics. *Small* **2021**, *17*, 2006054. [[CrossRef](#)]
100. Yu, S.; Tang, H.; Zhang, D.; Wang, S.; Qiu, M.; Song, G.; Fu, D.; Hu, B.; Wang, X. MXenes as emerging nanomaterials in water purification and environmental remediation. *Sci. Total Environ.* **2021**, *811*, 152280. [[CrossRef](#)] [[PubMed](#)]
101. Zhang, Y.; Xia, W.; Wu, Y.; Zhang, P. Prediction of MXene based 2D tunable band gap semiconductors: GW quasiparticle calculations. *Nanoscale* **2019**, *11*, 3993–4000. [[CrossRef](#)] [[PubMed](#)]
102. Thakur, R.; VahidMohammadi, A.; Moncada, J.; Adams, W.R.; Chi, M.; Tatarchuk, B.; Beidaghi, M.; Carrero, C.A. Insights into the thermal and chemical stability of multilayered V₂CT_x MXene. *Nanoscale* **2019**, *11*, 10716–10726. [[CrossRef](#)] [[PubMed](#)]
103. Seredych, M.; Shuck, C.E.; Pinto, D.; Alhabeib, M.; Precetti, E.; Deysher, G.; Anasori, B.; Kurra, N.; Gogotsi, Y. High-temperature behavior and surface chemistry of carbide MXenes studied by thermal analysis. *Chem. Mater.* **2019**, *31*, 3324–3332. [[CrossRef](#)]
104. Naguib, M.; Mashtalir, O.; Carle, J.; Presser, V.; Lu, J.; Hultman, L.; Gogotsi, Y.; Barsoum, M.W. Two-Dimensional Transition Metal Carbides. *ACS Nano* **2012**, *6*, 1322–1331. [[CrossRef](#)] [[PubMed](#)]
105. Koyappayil, A.; Chavan, S.G.; Roh, Y.-G.; Lee, M.-H. Advances of MXenes; Perspectives on Biomedical Research. *Biosensors* **2022**, *12*, 454. [[CrossRef](#)]
106. He, T.; Liu, W.; Lv, T.; Ma, M.; Liu, Z.; Vasiliev, A.; Li, X. MXene/SnO₂ heterojunction based chemical gas sensors. *Sens. Actuators B Chem.* **2021**, *329*, 129275. [[CrossRef](#)]
107. Zhao, F.; Yao, Y.; Jiang, C.; Shao, Y.; Barceló, D.; Ying, Y.; Ping, J. Self-reduction bimetallic nanoparticles on ultrathin MXene nanosheets as functional platform for pesticide sensing. *J. Hazard. Mater.* **2020**, *384*, 121358. [[CrossRef](#)]
108. Liu, X.; Qiu, Y.; Jiang, D.; Li, F.; Gan, Y.; Zhu, Y.; Pan, Y.; Wan, H.; Wang, P. Covalently grafting first-generation PAMAM dendrimers onto MXenes with self-adsorbed AuNPs for use as a functional nanoplatform for highly sensitive electrochemical biosensing of cTnT. *Microsyst. Nanoeng.* **2022**, *8*, 35. [[CrossRef](#)]
109. Medetalibeyoglu, H.; Kotan, G.; Atar, N.; Yola, M.L. A novel and ultrasensitive sandwich-type electrochemical immunosensor based on delaminated MXene@AuNPs as signal amplification for prostate specific antigen (PSA) detection and immunosensor validation. *Talanta* **2020**, *220*, 121403. [[CrossRef](#)]

110. Laochai, T.; Yukird, J.; Promphet, N.; Qin, J.; Chailapakul, O.; Rodthongkum, N. Non-invasive electrochemical immunosensor for sweat cortisol based on L-cys/AuNPs/MXene modified thread electrode. *Biosens. Bioelectron.* **2022**, *203*, 114039. [[CrossRef](#)] [[PubMed](#)]
111. Jiang, B.; Li, C.; Dag, Ö.; Abe, H.; Takei, T.; Imai, T.; Hossain, M.; Shahriar, A.; Islam, M.; Wood, K. Mesoporous metallic rhodium nanoparticles. *Nat. Commun.* **2017**, *8*, 15581. [[CrossRef](#)] [[PubMed](#)]
112. Liu, C.; Yang, W.; Min, X.; Zhang, D.; Fu, X.; Ding, S.; Xu, W. An enzyme-free electrochemical immunosensor based on quaternary metallic/nonmetallic PdPtBP alloy mesoporous nanoparticles/MXene and conductive CuCl₂ nanowires for ultrasensitive assay of kidney injury molecule-1. *Sens. Actuators B Chem.* **2021**, *334*, 129585. [[CrossRef](#)]
113. Yang, X.; Zhao, L.; Lu, L.; Feng, M.; Xia, J.; Zhang, F.; Wang, Z. In Situ Reduction of Gold Nanoparticle-Decorated Ti₃C₂ MXene for Ultrasensitive Electrochemical Detection of MicroRNA-21 with a Cascaded Signal Amplification Strategy. *J. Electrochem. Soc.* **2022**, *169*, 057505. [[CrossRef](#)]
114. Mohammadniaei, M.; Koyappayil, A.; Sun, Y.; Min, J.; Lee, M.-H. Gold nanoparticle/MXene for multiple and sensitive detection of oncomiRs based on synergetic signal amplification. *Biosens. Bioelectron.* **2020**, *159*, 112208. [[CrossRef](#)] [[PubMed](#)]
115. Wang, H.; Sun, J.; Lu, L.; Yang, X.; Xia, J.; Zhang, F.; Wang, Z. Competitive electrochemical aptasensor based on a cDNA-ferrocene/MXene probe for detection of breast cancer marker Mucin1. *Anal. Chim. Acta* **2020**, *1094*, 18–25. [[CrossRef](#)]
116. Cheng, J.; Hu, K.; Liu, Q.; Liu, Y.; Yang, H.; Kong, J. Electrochemical ultrasensitive detection of CYFRA21-1 using Ti₃C₂T_x-MXene as enhancer and covalent organic frameworks as labels. *Anal. Bioanal. Chem.* **2021**, *413*, 2543–2551. [[CrossRef](#)]
117. Wei, Y.; Zhang, P.; Soomro, R.A.; Zhu, Q.; Xu, B. Advances in the Synthesis of 2D MXenes. *Adv. Mater.* **2021**, *33*, 2103148. [[CrossRef](#)]
118. Wu, Q.; Li, Z.; Liang, Q.; Ye, R.; Guo, S.; Zeng, X.; Hu, J.; Li, A. Ultrasensitive electrochemical biosensor for microRNA-377 detection based on MXene-Au nanocomposite and G-quadruplex nano-amplification strategy. *Electrochim. Acta* **2022**, *428*, 140945. [[CrossRef](#)]
119. Liu, J.; Tang, D. Dopamine-loaded Liposomes-amplified Electrochemical Immunoassay Based on MXene (Ti₃C₂)–AuNPs. *Electroanalysis* **2022**, *34*, 1329–1337. [[CrossRef](#)]
120. Medetalibeyoglu, H.; Beytur, M.; Akyıldırım, O.; Atar, N.; Yola, M.L. Validated electrochemical immunosensor for ultra-sensitive procalcitonin detection: Carbon electrode modified with gold nanoparticles functionalized sulfur doped MXene as sensor platform and carboxylated graphitic carbon nitride as signal amplification. *Sens. Actuators B Chem.* **2020**, *319*, 128195. [[CrossRef](#)]
121. Liu, Y.; Zeng, H.; Chai, Y.; Yuan, R.; Liu, H. Ti₃C₂/BiVO₄ Schottky junction as a signal indicator for ultrasensitive photoelectrochemical detection of VEGF165. *Chem. Commun.* **2019**, *55*, 13729–13732. [[CrossRef](#)] [[PubMed](#)]
122. He, Y.; Zhou, W.; Qian, G.; Chen, B. Methane storage in metal–organic frameworks. *Chem. Soc. Rev.* **2014**, *43*, 5657–5678. [[CrossRef](#)] [[PubMed](#)]
123. Baumann, A.E.; Burns, D.A.; Liu, B.; Thoi, V.S. Metal-organic framework functionalization and design strategies for advanced electrochemical energy storage devices. *Commun. Chem.* **2019**, *2*, 86. [[CrossRef](#)]
124. Li, J.; Ye, W.; Chen, C. Chapter 5—Removal of toxic/radioactive metal ions by metal-organic framework-based materials. In *Interface Science and Technology*; Chen, C., Ed.; Elsevier: Amsterdam, The Netherlands, 2019; Volume 29, pp. 217–279.
125. Kreno, L.E.; Leong, K.; Farha, O.K.; Allendorf, M.; Van Duyne, R.P.; Hupp, J.T. Metal–organic framework materials as chemical sensors. *Chem. Rev.* **2012**, *112*, 1105–1125. [[CrossRef](#)]
126. James, S.L. Metal-organic frameworks. *Chem. Soc. Rev.* **2003**, *32*, 276–288. [[CrossRef](#)]
127. Johnson, E.M.; Ilic, S.; Morris, A.J. Design strategies for enhanced conductivity in metal–organic frameworks. *ACS Cent. Sci.* **2021**, *7*, 445–453. [[CrossRef](#)]
128. Escobar-Hernandez, H.U.; Pérez, L.M.; Hu, P.; Soto, F.A.; Papadaki, M.I.; Zhou, H.-C.; Wang, Q. Thermal Stability of Metal–Organic Frameworks (MOFs): Concept, Determination, and Model Prediction Using Computational Chemistry and Machine Learning. *Ind. Eng. Chem. Res.* **2022**, *61*, 5853–5862. [[CrossRef](#)]
129. Sun, Y.; Zhou, H.-C. Recent progress in the synthesis of metal–organic frameworks. *Sci. Technol. Adv. Mater.* **2015**, *16*, 054202. [[CrossRef](#)]
130. Dourandish, Z.; Tajik, S.; Beitollahi, H.; Jahani, P.M.; Nejad, F.G.; Sheikhshoaie, I.; Di Bartolomeo, A. A Comprehensive Review of Metal-Organic Framework: Synthesis, Characterization, and Investigation of Their Application in Electrochemical Biosensors for Biomedical Analysis. *Sensors* **2022**, *22*, 2238. [[CrossRef](#)]
131. Wu, L.-Z.; Zhou, X.-Y.; Zeng, P.-C.; Huang, J.-Y.; Zhang, M.-D.; Qin, L. Hydrothermal synthesis of Ni (II) or Co (II)-based MOF for electrocatalytic hydrogen evolution. *Polyhedron* **2022**, *225*, 116035. [[CrossRef](#)]
132. Wang, F.-X.; Wang, C.-C.; Du, X.; Li, Y.; Wang, F.; Wang, P. Efficient removal of emerging organic contaminants via photo-Fenton process over micron-sized Fe-MOF sheet. *Chem. Eng. J.* **2022**, *429*, 132495. [[CrossRef](#)]
133. Menon, S.S.; Chandran, S.V.; Koyappayil, A.; Berchmans, S. Copper- Based Metal-Organic Frameworks as Peroxidase Mimics Leading to Sensitive H₂O₂ and Glucose Detection. *ChemistrySelect* **2018**, *3*, 8319–8324. [[CrossRef](#)]
134. Nazari, Z.; Taher, M.A.; Fazelirad, H. A Zn based metal organic framework nanocomposite: Synthesis, characterization and application for preconcentration of cadmium prior to its determination by FAAS. *RSC Adv.* **2017**, *7*, 44890–44895. [[CrossRef](#)]
135. Ban, Y.; Li, Y.; Liu, X.; Peng, Y.; Yang, W. Solvothermal synthesis of mixed-ligand metal–organic framework ZIF-78 with controllable size and morphology. *Microporous Mesoporous Mater.* **2013**, *173*, 29–36. [[CrossRef](#)]

136. Liu, Y.; Wei, Y.; Liu, M.; Bai, Y.; Wang, X.; Shang, S.; Chen, J.; Liu, Y. Electrochemical Synthesis of Large Area Two-Dimensional Metal–Organic Framework Films on Copper Anodes. *Angew. Chem. Int. Ed.* **2021**, *60*, 2887–2891. [[CrossRef](#)]
137. Asghar, A.; Iqbal, N.; Noor, T.; Kariuki, B.M.; Kidwell, L.; Easun, T.L. Efficient electrochemical synthesis of a manganese-based metal–organic framework for H₂ and CO₂ uptake. *Green Chem.* **2021**, *23*, 1220–1227. [[CrossRef](#)]
138. Tang, D.; Yang, X.; Wang, B.; Ding, Y.; Xu, S.; Liu, J.; Peng, Y.; Yu, X.; Su, Z.; Qin, X. One-Step Electrochemical Growth of 2D/3D Zn(II)-MOF Hybrid Nanocomposites on an Electrode and Utilization of a PtNPs@2D MOF Nanocatalyst for Electrochemical Immunoassay. *ACS Appl. Mater. Interfaces* **2021**, *13*, 46225–46232. [[CrossRef](#)]
139. Wu, W.; Decker, G.E.; Weaver, A.E.; Arnoff, A.I.; Bloch, E.D.; Rosenthal, J. Facile and Rapid Room-Temperature Electrosynthesis and Controlled Surface Growth of Fe-MIL-101 and Fe-MIL-101-NH₂. *ACS Cent. Sci.* **2021**, *7*, 1427–1433. [[CrossRef](#)]
140. Ghoorchian, A.; Afkhami, A.; Madrakian, T.; Ahmadi, M. Chapter 9—Electrochemical synthesis of MOFs. In *Metal–Organic Frameworks for Biomedical Applications*; Mozafari, M., Ed.; Woodhead Publishing: Cambridge, UK, 2020; pp. 177–195.
141. Ameloot, R.; Stappers, L.; Franssaer, J.; Alaerts, L.; Sels, B.F.; De Vos, D.E. Patterned growth of metal-organic framework coatings by electrochemical synthesis. *Chem. Mater.* **2009**, *21*, 2580–2582. [[CrossRef](#)]
142. Bazzi, L.; Ayouch, I.; Tachallait, H.; Hankari, S.E.L. Ultrasound and microwave assisted-synthesis of ZIF-8 from zinc oxide for the adsorption of phosphate. *Results Eng.* **2022**, *13*, 100378. [[CrossRef](#)]
143. Koyappayil, A.; Yeon, S.-h.; Chavan, S.G.; Jin, L.; Go, A.; Lee, M.-H. Efficient and rapid synthesis of ultrathin nickel-metal organic framework nanosheets for the sensitive determination of glucose. *Microchem. J.* **2022**, *179*, 107462. [[CrossRef](#)]
144. Lee, J.H.; Ahn, Y.; Kwak, S.-Y. Facile Sonochemical Synthesis of Flexible Fe-Based Metal–Organic Frameworks and Their Efficient Removal of Organic Contaminants from Aqueous Solutions. *ACS Omega* **2022**, *7*, 23213–23222. [[CrossRef](#)]
145. Li, J.; Liu, L.; Ai, Y.; Liu, Y.; Sun, H.; Liang, Q. Self-Polymerized Dopamine-Decorated Au NPs and Coordinated with Fe-MOF as a Dual Binding Sites and Dual Signal-Amplifying Electrochemical Aptasensor for the Detection of CEA. *ACS Appl. Mater. Interfaces* **2020**, *12*, 5500–5510. [[CrossRef](#)] [[PubMed](#)]
146. Li, W.; Yang, Y.; Ma, C.; Song, Y.; Hong, C.; Qiao, X. A sandwich-type electrochemical immunosensor for ultrasensitive detection of CEA based on core–shell Cu₂O@Cu-MOF@Au NPs nanostructure attached with HRP for triple signal amplification. *J. Mater. Sci.* **2020**, *55*, 13980–13994. [[CrossRef](#)]
147. Mulchandani, A.; Myung, N.V. Conducting polymer nanowires-based label-free biosensors. *Curr. Opin. Biotechnol.* **2011**, *22*, 502–508. [[CrossRef](#)]
148. Zhang, Y.; Kolmakov, A.; Lilach, Y.; Moskovits, M. Electronic Control of Chemistry and Catalysis at the Surface of an Individual Tin Oxide Nanowire. *J. Phys. Chem. B* **2005**, *109*, 1923–1929. [[CrossRef](#)]
149. Li, S.; Yue, S.; Yu, C.; Chen, Y.; Yuan, D.; Yu, Q. A label-free immunosensor for the detection of nuclear matrix protein-22 based on a chrysanthemum-like Co-MOFs/CuAu NWs nanocomposite. *Analyst* **2019**, *144*, 649–655. [[CrossRef](#)]
150. Feng, J.; Wang, H.; Ma, Z. Ultrasensitive amperometric immunosensor for the prostate specific antigen by exploiting a Fenton reaction induced by a metal-organic framework nanocomposite of type Au/Fe-MOF with peroxidase mimicking activity. *Microchim. Acta* **2020**, *187*, 95. [[CrossRef](#)]
151. Mehmandoust, M.; Erk, E.E.; Soylak, M.; Erk, N.; Karimi, F. Metal–Organic Framework Based Electrochemical Immunosensor for Label-Free Detection of Glial Fibrillary Acidic Protein as a Biomarker. *Ind. Eng. Chem. Res.* **2022**. [[CrossRef](#)]
152. Zhao, S.; Zhang, Y.; Ding, S.; Fan, J.; Luo, Z.; Liu, K.; Shi, Q.; Liu, W.; Zang, G. A highly sensitive label-free electrochemical immunosensor based on AuNPs-PtNPs-MOFs for nuclear matrix protein 22 analysis in urine sample. *J. Electroanal. Chem.* **2019**, *834*, 33–42. [[CrossRef](#)]
153. Joseph, J.; Iftekhar, S.; Srivastava, V.; Fallah, Z.; Zare, E.N.; Sillanpää, M. Iron-based metal-organic framework: Synthesis, structure and current technologies for water reclamation with deep insight into framework integrity. *Chemosphere* **2021**, *284*, 131171. [[CrossRef](#)] [[PubMed](#)]
154. Silva, P.; Vilela, S.M.F.; Tomé, J.P.C.; Almeida Paz, F.A. Multifunctional metal–organic frameworks: From academia to industrial applications. *Chem. Soc. Rev.* **2015**, *44*, 6774–6803. [[CrossRef](#)]
155. Wang, W.; Yu, Y.; Jin, Y.; Liu, X.; Shang, M.; Zheng, X.; Liu, T.; Xie, Z. Two-dimensional metal-organic frameworks: From synthesis to bioapplications. *J. Nanobiotechnol.* **2022**, *20*, 207. [[CrossRef](#)]
156. Cheng, T.; Li, X.; Huang, P.; Wang, H.; Wang, M.; Yang, W. Colorimetric and electrochemical (dual) thrombin assay based on the use of a platinum nanoparticle modified metal-organic framework (type Fe-MIL-88) acting as a peroxidase mimic. *Microchim. Acta* **2019**, *186*, 94. [[CrossRef](#)]
157. Sun, D.; Luo, Z.; Lu, J.; Zhang, S.; Che, T.; Chen, Z.; Zhang, L. Electrochemical dual-aptamer-based biosensor for nonenzymatic detection of cardiac troponin I by nanohybrid electrocatalysts labeling combined with DNA nanotetrahedron structure. *Biosens. Bioelectron.* **2019**, *134*, 49–56. [[CrossRef](#)]
158. Miao, J.; Du, K.; Li, X.; Xu, X.; Dong, X.; Fang, J.; Cao, W.; Wei, Q. Ratiometric electrochemical immunosensor for the detection of procalcitonin based on the ratios of SiO₂-Fc-COOH–Au and UiO-66-TB complexes. *Biosens. Bioelectron.* **2021**, *171*, 112713. [[CrossRef](#)]
159. Dong, H.; Liu, S.; Liu, Q.; Li, Y.; Li, Y.; Zhao, Z. A dual-signal output electrochemical immunosensor based on Au–MoS₂/MOF catalytic cycle amplification strategy for neuron-specific enolase ultrasensitive detection. *Biosens. Bioelectron.* **2022**, *195*, 113648. [[CrossRef](#)]

160. Wang, S.; Wang, M.; Li, C.; Li, H.; Ge, C.; Zhang, X.; Jin, Y. A highly sensitive and stable electrochemiluminescence immunosensor for alpha-fetoprotein detection based on luminol-AgNPs@Co/Ni-MOF nanosheet microflowers. *Sens. Actuators B Chem.* **2020**, *311*, 127919. [[CrossRef](#)]
161. Du, D.; Shu, J.; Guo, M.; Haghighatbin, M.A.; Yang, D.; Bian, Z.; Cui, H. Potential-Resolved Differential Electrochemiluminescence Immunosensor for Cardiac Troponin I Based on MOF-5-Wrapped CdS Quantum Dot Nanoluminophores. *Anal. Chem.* **2020**, *92*, 14113–14121. [[CrossRef](#)]
162. Dai, L.; Li, Y.; Wang, Y.; Luo, X.; Wei, D.; Feng, R.; Yan, T.; Ren, X.; Du, B.; Wei, Q. A prostate-specific antigen electrochemical immunosensor based on Pd NPs functionalized electroactive Co-MOF signal amplification strategy. *Biosens. Bioelectron.* **2019**, *132*, 97–104. [[CrossRef](#)] [[PubMed](#)]
163. Gao, X.; Liu, H.; Wang, D.; Zhang, J. Graphdiyne: Synthesis, properties, and applications. *Chem. Soc. Rev.* **2019**, *48*, 908–936. [[CrossRef](#)] [[PubMed](#)]
164. Hou, Y.-Y.; Xu, J.; Wang, F.-T.; Dong, Z.; Tan, X.; Huang, K.-J.; Li, J.-Q.; Zuo, C.-Y.; Zhang, S.-Q. Construction of an Integrated Device of a Self-Powered Biosensor and Matching Capacitor Based on Graphdiyne and Multiple Signal Amplification: Ultrasensitive Method for MicroRNA Detection. *Anal. Chem.* **2021**, *93*, 15225–15230. [[CrossRef](#)] [[PubMed](#)]
165. Pourali, A.; Rashidi, M.R.; Barar, J.; Pavon-Djavid, G.; Omid, Y. Voltammetric biosensors for analytical detection of cardiac troponin biomarkers in acute myocardial infarction. *TrAC-Trends Anal. Chem.* **2021**, *134*, 116123. [[CrossRef](#)]
166. Adeel, M.; Rahman, M.M.; Lee, J.-J. Label-free aptasensor for the detection of cardiac biomarker myoglobin based on gold nanoparticles decorated boron nitride nanosheets. *Biosens. Bioelectron.* **2019**, *126*, 143–150. [[CrossRef](#)]
167. Cohen, M.L. Calculation of bulk moduli of diamond and zinc-blende solids. *Phys. Rev. B* **1985**, *32*, 7988–7991. [[CrossRef](#)]
168. Liu, A.Y.; Cohen, M.L. Prediction of New Low Compressibility Solids. *Science* **1989**, *245*, 841–842. [[CrossRef](#)]
169. Zhu, J.; Xiao, P.; Li, H.; Carabineiro, S.A.C. Graphitic Carbon Nitride: Synthesis, Properties, and Applications in Catalysis. *ACS Appl. Mater. Interfaces* **2014**, *6*, 16449–16465. [[CrossRef](#)]
170. Bott Neto, J.L.; Martins, T.S.; Machado, S.A.; Oliveira, O.N. Enhanced photocatalysis on graphitic carbon nitride sensitized with gold nanoparticles for photoelectrochemical immunosensors. *Appl. Surf. Sci.* **2022**, *606*, 154952. [[CrossRef](#)]
171. Wu, Z.; Lyu, Y.; Zhang, Y.; Ding, R.; Zheng, B.; Yang, Z.; Lau, S.P.; Chen, X.H.; Hao, J. Large-scale growth of few-layer two-dimensional black phosphorus. *Nat. Mater.* **2021**, *20*, 1203–1209. [[CrossRef](#)]
172. Gaufres, E.; Fossard, F.; Gosselin, V.; Sponza, L.; Ducastelle, F.; Li, Z.; Louie, S.G.; Martel, R.; Côté, M.; Loiseau, A. Momentum-resolved dielectric response of free-standing mono-, bi-, and trilayer black phosphorus. *Nano Lett.* **2019**, *19*, 8303–8310. [[CrossRef](#)]
173. Youngblood, N.; Chen, C.; Koester, S.J.; Li, M. Waveguide-integrated black phosphorus photodetector with high responsivity and low dark current. *Nat. Photonics* **2015**, *9*, 247–252. [[CrossRef](#)]
174. Wu, Z.; Hao, J. Electrical transport properties in group-V elemental ultrathin 2D layers. *NPJ 2D Mater. Appl.* **2020**, *4*, 4. [[CrossRef](#)]
175. Li, Z.; Fu, Y.; Zhu, Q.; Wei, S.; Gao, J.; Zhu, Y.; Xue, T.; Bai, L.; Wen, Y. High-stable Phosphorene-supported Bimetallic Pt-Pd Nanoelectrocatalyst for p-Aminophenol, β -Galactosidase, and Escherichia coli. *Int. J. Electrochem. Sci* **2020**, *15*, 3089–3103. [[CrossRef](#)]
176. Shanmuganathan, K.; Ellison, C.J. Chapter 20—Layered Double Hydroxides: An Emerging Class of Flame Retardants. In *Polymer Green Flame Retardants*; Paspaspyrides, C.D., Kiliaris, P., Eds.; Elsevier: Amsterdam, The Netherlands, 2014; pp. 675–707.
177. Wu, M.; Liu, S.; Qi, F.; Qiu, R.; Feng, J.; Ren, X.; Rong, S.; Ma, H.; Chang, D.; Pan, H. A label-free electrochemical immunosensor for CA125 detection based on CMK-3(Au/Fc@MgAl-LDH)_n multilayer nanocomposites modification. *Talanta* **2022**, *241*, 123254. [[CrossRef](#)]
178. Ojha, R.P.; Singh, P.; Azad, U.P.; Prakash, R. Impedimetric immunosensor for the NS1 dengue biomarker based on the gold nanorod decorated graphitic carbon nitride modified electrode. *Electrochim. Acta* **2022**, *411*, 140069. [[CrossRef](#)]
179. Jalal, U.M.; Jin, G.J.; Shim, J.S. Paper-Plastic Hybrid Microfluidic Device for Smartphone-Based Colorimetric Analysis of Urine. *Anal. Chem.* **2017**, *89*, 13160–13166. [[CrossRef](#)]
180. Chung, S.; Breshears, L.E.; Perea, S.; Morrison, C.M.; Betancourt, W.Q.; Reynolds, K.A.; Yoon, J.Y. Smartphone-Based Paper Microfluidic Particulometry of Norovirus from Environmental Water Samples at the Single Copy Level. *ACS Omega* **2019**, *4*, 11180–11188. [[CrossRef](#)]

Disclaimer/Publisher's Note: The statements, opinions and data contained in all publications are solely those of the individual author(s) and contributor(s) and not of MDPI and/or the editor(s). MDPI and/or the editor(s) disclaim responsibility for any injury to people or property resulting from any ideas, methods, instructions or products referred to in the content.